Tailoring T_{fh} Profiles Enhances Antibody Persistence to a Clade C HIV-1 Vaccine in Rhesus Macaques

Anil Verma[1*], Chase E Hawes[2,3*], Sonny R Elizaldi[2,4], Justin C. Smith[5], Dhivyaa Rajasundaram[6], Gabriel Kristian Pedersen[7], Xiaoying Shen[8,9], LaTonya D Williams[8,9,10], Georgia D. Tomaras[8,9,10,11], Pamela A. Kozlowski[5], Rama R. Amara[12,13], Smita S. Iyer[1,3,4]

[1]Department of Pathology, School of Medicine, University of Pittsburgh, PA; [2]Graduate Group in Immunology, UC Davis, Davis, CA; [3]California National Primate Research Center, UC Davis, CA; [4]Department of Pathology, Microbiology, and Immunology, School of Veterinary Medicine, UC Davis, CA; [5]Department of Microbiology, Immunology, and Parasitology, Louisiana State University Health Sciences Center, New Orleans, LA; [6]Department of Pediatrics, School of Medicine, University of Pittsburgh, PA;[7] Statens Serum Institut, Copenhagen, DK-2300, Denmark; [8]Duke Human Vaccine Institute, Duke University Medical Center, Durham, NC; Departments of [9]Surgery, [10]Medicine,[11]Molecular Genetics and Microbiology, and Immunology, Duke University Medical Center, Durham, NC; [12]Department of Microbiology and Immunology, Emory University, Atlanta, Georgia, USA; [13] Emory National Primate Research Center, Emory University, Atlanta, GA

*Authors contributed equally

Corresponding author/Lead contact: siyer.3@pitt.edu

ABSTRACT

CD4 T follicular helper cells (T_{fh}) are essential for establishing serological memory and have distinct helper attributes that impact both the quantity and quality of the antibody response. Insights into T_{fh} subsets that promote antibody persistence and functional capacity can critically inform vaccine design. Based on the T_{fh} profiles evoked by the live attenuated measles virus vaccine, renowned for its ability to establish durable humoral immunity, we investigated the potential of a T_{fh}1/17 recall response during the boost phase to enhance persistence of HIV-1 Envelope (Env) antibodies in rhesus macaques. Using a DNA-prime encoding gp160 antigen and T_{fh} polarizing cytokines (interferon protein-10 (IP-10) and interleukin-6 (IL-6)), followed by a gp140 protein boost formulated in a cationic liposome-based adjuvant (CAF01), we successfully generated germinal center (GC) T_{fh}1/17 cells. In contrast, a similar DNA-prime (including IP-10) followed by gp140 formulated with monophosphoryl lipid A (MPLA)+QS-21 adjuvant predominantly induced GC T_{fh}1 cells. While the generation of GC T_{fh}1/17 cells with CAF01 and GC T_{fh}1 cells with MPLA+QS-21 induced comparable peak Env antibodies, the latter group demonstrated significantly greater antibody concentrations at week 8 after final immunization which persisted up to 30 weeks (gp140 IgG ng/ml- MPLA; 5500; CAF01, 2155; $p < 0.05$). Notably, interferon γ+ Env-specific T_{fh} responses were consistently higher with gp140 in MPLA+QS-21 and positively correlated with Env antibody persistence. These findings suggest that vaccine platforms maximizing GC T_{fh}1 induction promote persistent Env antibodies, important for protective immunity against HIV.

INTRODUCTION

Despite options for testing and treatment, progress against HIV is slowing, emphasizing the urgent need for an HIV vaccine(Fauci 2017, Eisinger and Fauci 2018). While advances have been made in immunogen design and vaccine approaches, the main challenge lies in generating durable, high-affinity antibodies against the HIV-1 Envelope (Env) glycoprotein, crucial for protection. To design a vaccine that confers long-term protective immunity, effective stimulation of CD4 T follicular helper (T_{fh}) cells is essential, as they provide vital costimulatory and cytokine support to B cells within germinal centers (GC), leading to the production of persistent antibodies following immunization (Slifka, Antia et al. 1998, Crotty 2014). T_{fh} cells possess distinctive T_h1, T_h2, and T_h17-type cell attributes, programmed by the inflammatory response during the T-cell priming phase, with each T_{fh} subset differentially contributing to GC B cell proliferation, survival, and differentiation (Morita, Schmitt et al. 2011, Barbet, Sander et al. 2018) (Gao, Luo et al. 2023). Therefore, in addition to antigen selection, promoting the differentiation and expansion of optimal T_{fh} subsets to generate potent and enduring humoral immunity is critical for vaccine design.

Guiding the type of adaptive response to produce the most effective forms of immunity for each specific pathogen achieve qualitative alteration of the immune response. For vaccines currently under development, adjuvants are increasingly used to promote types of immunity not effectively generated by the nonadjuvanted antigens. For example, adjuvants have been used in preclinical and clinical studies to: (1) provide functionally appropriate types of immune response (e.g., T helper 1 [Th1] cell versus Th2 cell, $CD8^+$ versus $CD4^+$ T cells, specific antibody isotypes).

Clinical studies have demonstrated that booster immunization with a T_h1 glucopyranosyl lipid adjuvant-stable emulsion (GLA-SE)-formulated malaria antigen leads to enhanced antibodies at memory time points compared to an aluminum adjuvanted vaccine(Hill, Pierson et al. 2019).

We demonstrated that promoting the induction of $T_{fh}1$ cells by utilizing interferon-induced protein (IP)10, a ligand for and an inducer of CXCR3, as a molecular adjuvant to a DNA vaccine (DNA_{IP10}) followed by boosting with protein adjuvanted with Army Liposome Formulation (ALFQ) consisting

85 of liposomal monophosphoryl lipid A (MPLA) plus a saponin derivative, QS-21 (Alving, Peachman
86 et al. 2012, Rao, Onkar et al. 2018) enhanced GC responses, increased HIV anti-Env binding
87 antibodies, and stimulated significantly higher cross-clade reactivity with increased specificity to
88 V1V2 conformational epitopes, and higher avidity (Verma, Schmidt et al. 2019). Similarly, a recent
89 macaque study utilizing Clade C DNA+GLA-SE adjuvanted Env protein immunization revealed
90 that frequencies of Env-specific CD28+ IFNγ+ cells, indicative of T_h1 responses, correlated with
91 the development of Env antibodies following the final immunization (Felber, Lu et al. 2020).
92
93 In addition to IFNγ, interleukin 17 (IL-17) has been shown to enhance cognate T-B cell
94 interactions, leading to an effective GC response (Moyron-Quiroz, Rangel-Moreno et al. 2004,
95 Mitsdoerffer, Lee et al. 2010, Kumar, Chen et al. 2013). Studies conducted in mice have further
96 demonstrated that $T_{fh}17$ cells support efficient antibody recall responses (Gao, Luo et al. 2023).
97 Notably, the persistence of peripheral $T_{fh}17$ cells specific to measles has been observed in adults
98 who have received the live attenuated measles virus vaccine (LAMV) during childhood,
99 suggesting that measles vaccine triggers $T_{fh}17$ responses which persist beyond the GC phase
100 (Gao, Luo et al. 2023). Intriguingly, earlier studies exploring peripheral CD4 T cell determinants
101 of serological memory elicited by LAMV have led to the hypothesis that LAMV promotes both T_h1
102 and T_h2 CD4 differentiation programs, based on production of $IFN\gamma^+$ and IL-4, which are cytokines
103 also produced by T_{fh} cells (Ovsyannikova, Dhiman et al. 2003) (Ward and Griffin 1993,
104 Ovsyannikova, Reid et al. 2003). However, our understanding of the GC T_{fh} cell response to
105 LAMV, which plays a crucial role in establishing long-term immunity against measles, remains
106 incomplete.
107
108 In this study, based on GC T_{fh} profiles evoked by LAMV, we explored the potential of a $T_{fh}1$ or
109 mixed $T_{fh}1/17$ targeted vaccine to enhance HIV-1 Env antibodies in rhesus macaques using an
110 DNA-prime/protein boost approach. After booster immunization with a Clade C gp140 protein

formulated in CAF01(Wørzner, Hvannastein et al. 2021), a cationic liposome-based formulation, we observed the generation of $T_{fh}1/17$ cells within GCs, while $T_{fh}1$ cells were induced when monophosphoryl lipid A (MPLA)+QS-21 was used as the adjuvant. Notably, stimulating $T_{fh}1$ cell induction with MPLA resulted in significantly greater antibody persistence at week 8 and up to 30 weeks after the final immunization. Moreover, the $T_{fh}1$ regimen with MPLA adjuvant led to higher tier 1 neutralization titers, increased levels of IgG1 subclass antibodies, and improved antibody effector functions. These findings highlight a unique potential of $T_{fh}1$ cells in promoting humoral immunity against HIV and suggest that vaccine strategies maximizing $T_{fh}1$ cell induction may hold promise for eliciting durable protective immunity against HIV.

138 **RESULTS**

139 **GC T_{fh}1 and GC T_{fh}17 cells recalled by measles booster.**

140 To decipher the specific T_h subset of T_{fh} cells contributing to the establishment of durable
141 serological memory, we employed live attenuated measles virus vaccine (LAMV) as a model and
142 investigated T_{fh} responses in peripheral blood and lymph nodes (LN) in a cohort of 16 healthy
143 adult female rhesus macaques (**Figure 1A**). Consistent with documented evidence of long-term
144 persistence of the memory B cell response to LAMV, rapid recall of measles virus (MeV) IgG
145 ensued at week 2 post LAMV, irrespective of the booster interval (**Figure 1B**). By week 20, MeV
146 IgG concentrations displayed a 2.6-fold increase compared to baseline, signifying the efficacy of
147 LAMV booster in generating persistent antibodies. These augmented levels of memory antibodies
148 were accompanied by enhanced antibody avidity (**Figure 1C)**, underscoring robustness of the
149 humoral immune response elicited by LAMV.

150

151 Tracking MeV-specific T_{fh} cells using the activation-induced marker (AIM) assay showed induction
152 of peripheral (p)T_{fh} cells at day 7 post-vaccination (**Fig Supplementary Figure 1A**). Confirming
153 T_{fh} cell induction in response to LAMV, activated pT_{fh} cells, identified by co-expression of ICOS
154 and Ki-67, were transiently upregulated at day 7 (**Fig 1D, Supplementary Figure 1B**). These
155 responding pT_{fh} cells were PD-1+ and their frequencies at day 7, but not day 0, significantly
156 correlated with MeV IgG at Week 20 (**Fig 1E**). We next proceeded to analyze heterogeneity within
157 pT_{fh} cells with respect to expression of T_h1/2/17 chemokine receptors. Our temporal analysis of
158 the responding pT_{fh} compartment demonstrated significant induction of CXCR3+ T_{fh}1 cells at day
159 7 (**Fig 1F**). In contrast, we observed a decrease in frequencies of CCR4-expresisng pT_{fh}2 subsets
160 and CCR6-expressing pT_{fh}17 subsets. Utilizing Boolean analysis, we further identified that the
161 majority of responding pT_{fh} cells expressed CXCR3, indicating induction of pT_{fh}1 cells in response
162 to LAMV (**Fig 1G**).

163

164 Expanding our investigation to include phenotypic and molecular features of CXCR5^{+} PD-1^{++} GC
165 T_{fh} cells (**Fig 1H, Supplementary Figure 1C),** we found predominance of CXCR3 expression
166 within the GC T_{fh} population. Additionally, we observed that up to 25% of GC T_{fh} cells expressed
167 CCR6. Notably, our analysis did not reveal substantial expression of CCR4 within GC T_{fh} cells.
168 Molecular analysis of sorted CXCR5+ PD-1+/++ LN T_{fh} cells (**Supplementary Figure 1D**) further
169 provided insights into their functional specialization, with the induction of key transcription factors
170 BATF and IRF4, as well as the expression of chemokine receptors CCR5 and CCR6, indicating
171 the activation of T_h1 and T_h17 programs within GC T_{fh} cells (**Figure 1J-K**). Collectively, these
172 findings demonstrate that both blood and GC T_{fh} cells, during the peak effector response following
173 LAMV immunization, exhibit a predominant $T_{fh}1$ helper bias, with GC T_{fh} cells also demonstrating
174 a $T_{fh}17$ bias.
175
176 **HIV-1 vaccine modalities for inducing GC $T_{fh}1$ and GC $T_{fh}17$ subsets.**
177 Building on our observations made with LAMV, we next investigated the potential of fine-tuning
178 T_{fh} responses towards $T_{fh}1$ and $T_{fh}17$ profiles for generation of persistent anti-HIV-1 Env
179 antibodies. We immunized two cohorts of rhesus macaques against HIV Env using a DNA prime
180 and protein boost vaccination strategy tailored towards either a $T_{fh}1$ (n=6) or mixed $T_{fh}1/17$ (n=6)
181 response (**Figure Supplementary Figure 2**). For both vaccine regimens, animals received an
182 initial intradermal DNA prime vaccine encoding HIV-1 Env gp160 (C.1086C) at weeks 0, 4, 8,
183 followed by an subcutaneous HIV C.ZA 1197MB Env gp140 protein boost vaccination at weeks
184 12 and 20. To tailor vaccine induced T_{fh} responses, we included additional T_{fh} polarizing factors
185 with DNA prime vaccines encoding for cytokines IP-10 ($T_{fh}1$ regimen) or IP-10 and IL-6 (mixed
186 $T_{fh}1/17$ regimen), coupled with corresponding gp140 protein boost formulated in either the T_h1
187 polarizing adjuvants, MPLA+QS-21, or the $T_h1/17$ polarizing CAF01 adjuvant platform,
188 respectively. Over the course of both the priming and boost stages, we performed routine
189 collection of both blood and rectal secretions from animals to assess the extent of systemic and

190 mucosal humoral immunity elicited by the two regimens. Additionally, we collected inguinal LN
191 biopsies and fine needle aspirates of LN (FNA) at baseline, during the DNA prime stage, and
192 following both protein boost to comprehensively characterize vaccine-elicited GC T_{fh} responses
193 in draining LNs. GC responses typically peak between 2-3 weeks post first booster with more
194 rapid recall kinetics after the second booster (Iyer, Gangadhara et al. 2015). Our rationale for
195 sampling LN 3 weeks following the 2nd booster was to assess whether the reported effects of
196 CAF01 on sustained antigen release might result in GC persistence (Henriksen-Lacey,
197 Christensen et al. 2011, Pedersen, Wørzner et al. 2020).
198
199 **Induction of Robust T Cell Activation in GCs with HIV-1 Env Formulated in CAF01 and**
200 **MPLA+QS-21 Adjuvants.**
201 To gain insights into LN T_{fh} responses induced by MPLA and CAF01 platforms, we utilized
202 complementary approaches of situ protein expression analysis of GCs and RNA sequencing of
203 Env-stimulated CD95+ CD4 T cells of selected animals in each vaccine group (**Figure 2A**).To
204 track immunological changes within GCs, we applied the GeoMx Digital Spatial Profiler to assess
205 protein expression of key immune targets longitudinally at baseline (BL, prior to DNA
206 immunization), week 2 of protein 1 (P1w2) and week 3 of protein 2 (P2w3). We stained tissue
207 sections with morphological markers (CD20, CD3, Ki-67) and collected circular regions of interest
208 (ROI) based on co-localization of CD3 with CD20+ Ki-67+ GC B cells. For each tissue, two to
209 three ROIs were selected to ensure adequate representation of GCs within each animal. This
210 approach allowed us to accurately identify GCs and analyze protein expression of both T and B
211 cells within these specific regions (**Figure 2B**).
212
213 Thirty-two protein targets were profiled simultaneously, along with isotype controls (Ms IgG1, Ms
214 IgG2A, Rb IgG) and housekeeping proteins (S6, Histone H3, GAPDH). After applying quality
215 control measures, we calculated the signal-to-noise ratio for each target which provided robust

216 assessment of protein expression levels (**Supplementary Figure 3A-D**). CD45 and B2M were
217 among the most abundantly expressed proteins while LAG3 and PD-L1 demonstrated low signal
218 expression. To address variations in ROI surface area and tissue quality, normalized protein
219 expression (NPE) was calculated for each protein. NPE analysis revealed robust expression of
220 key lineage proteins, CD45, CD20, CD3, CD4, and CD8, as well as GC markers PD-1 and Ki-67
221 within ROIs (**Figure 2C**). We observed notable associations between protein expression patterns
222 within the GC microenvironment; specifically, a strong correlation between the expression of CD4
223 and CD20 was observed (**Supplementary Figure 3E**). Furthermore, a significant association
224 between the co-stimulatory molecule 4-1BB and CD4 expression (**Supplementary Figure 3F**)
225 was observed within the GC. Association of the innate immune protein stimulator of interferon
226 genes (STING) with both 4-1BB and CD4 expression suggested a potential interplay between
227 innate and adaptive immune pathways within the context of GC responses. Altogether, the protein
228 expression data provide evidence for coordinated expression of key proteins involved in GC
229 function in both vaccine groups (**Supplementary Figure 3G)**.
230
231 To identify specific proteins and pathways activated in response to vaccination, we performed
232 differential expression analysis on a per-protein basis. We modeled NPE using a linear mixed-
233 effect model (LMM), which allowed us to account for sampling multiple ROIs per tissue within
234 each animal (FDR p value cut-off, < 0.05). Volcano plots illustrate proteins induced at P1w2
235 (**Figure 2D**) and P2w3 (**Figure 2E**) following vaccination. Induction of 4-1BB, ICOS, PD-1,
236 CD44 post boost indicated activation of T cells to antigen stimulation within GCs in both vaccine
237 groups (**Figure 2F**). The higher relative expression of these proteins at P2w3 was consistent
238 with the reported effects of CAF01 in GC persistence. We found that expression of the
239 checkpoint inhibitors CTLA4 and PD-L1 was significantly reduced post CAF01 vaccination,
240 while CD4 expression increased. In contrast, expression of the regulatory enzyme, IDO1;

241 checkpoint inhibitor, PD-L2; and CD256 (B7-H3), and the innate sensor, STING, was
242 significantly higher post vaccination in the MPLA group (**Figure 2D-E, G**).
243
244 Across vaccine regimens, significant differences were observed at P1w2 (**Figure 2H**).
245 Significantly higher expression of Ki-67 with MPLA compared to CAF01 was suggestive of a more
246 rapid GC response (**Figure 2H**). Furthermore, the check point inhibitory receptors LAG3, CTLA4,
247 as well as IDO1, exhibited higher expression levels with MPLA at P1w2. Importantly, no significant
248 differences were observed at BL, validating the specificity of immune activation to vaccination.
249 Altogether, the in-situ protein analysis indicated robust induction of GC responses across
250 vaccine platforms with distinct qualitative and quantitative effects initiated by MPLA versus
251 CAF01 suggesting potential differences in regulatory mechanisms and immune activation
252 pathways between the vaccine regimens.
253
254 **T_h1 molecular programs potentiated by HIV-1 Env/MPLA+QS-21.**
255 To assess the extent of T_h1/T_h17 programming in CD4 T cells induced by vaccination, we profiled
256 the transcriptome of CD95+ CD4 T cells isolated from the LN. We sort purified and RNA
257 sequenced naive (CD95-) and CD95+ CD4 T cells at BL, P1w2, and P2w3 following overnight
258 stimulation with HIV-1 Clade C Env peptide pools. A total of 18 samples per group, which
259 included three biological replicates per subset, were sequenced in parallel resulting in over 25
260 million high-quality reads per sample (**Figures 3A, Supplementary Figure S4A-B**). The
261 transcriptomes of naive versus CD95+ CD4 T cells post immunization, in alignment with their
262 distinctive biological states, exhibited clear demarcations along distinct dimensions within the
263 principal component analysis (PCA) plot (**Figure 3B**). Transcription factors (TF) involved in
264 regulating distinct cellular differentiation programs were enriched in CD95+ CD4 T cells at P1w2
265 and P2w3. These included HOPX, IKZF2, PRDM1, RUNX2, associated with effector
266 differentiation. Additionally, TF such as BATF, BCL6, BHLHE40, EGR2, and TOX2 involved in

267 T_{fh} differentiation were also identified. Furthermore, we identified genes regulating T_h1 (STAT1,
268 TBX21, EOMES), T_h17 (AHR), and Treg (FOXP3, NR4A2) programs. Moreover, the expression
269 of interferon regulatory factors (IRFs) controlling T cell differentiation (IRF1, IRF5, IRF8) was
270 observed, demonstrating that CD95+ cells post vaccination encompassed effector and fully
271 differentiated CD4 T cell subsets (**Figure 3C**).
272
273 We first assessed temporal changes in gene expression by focusing on differentially expressed
274 genes (DEGs) within CD95+ cells at P1w2 and P2w3, compared to BL (**Venn diagram in 3D**).
275 Notably, a significantly higher level of transcriptional perturbation was observed in response to
276 CAF01, particularly at P2w3, within both naive and CD95+ CD4 T cells (**top bubble plot in 3D,**
277 **S4C**), suggesting that CAF01 induces extensive gene expression changes in a cell-extrinsic
278 manner. By specifically examining genes induced exclusively in CD95+ cells, but not naive cells,
279 at P1w2, we made several observations. The T_h1 transcriptional regulator STAT1, as well as
280 IFNγ-induced genes such as IRF7, IRF8, IFI30, XAF-1, and CXCL11, were among the most
281 highly expressed genes in MPLA (**bottom bubble plot, 3D**), highlighting the activation of T_h1
282 programs following vaccination. Indeed, interrogation of top 3 eniched pathways utilizing the
283 Reactome database (Fabregat, Sidiropoulos et al. 2017) revealed that genes encompassing
284 IFNγ, IL-7, and IL-10 signaling networks were induced with MPLA at P1w2. In the CAF01 group,
285 we observed enrichment of co-stimulatory molecules TNFRSF8 (CD30) and TNFRS13B (TACI),
286 expressed by activated T cells, along with expression of the anti-apoptotic molecule BCL-2 and
287 the transcription factor Foxp3.
288
289 Analysis of genes downregulated showed pathways regulating cell cycle inhibitors p21 and p53
290 were enriched with MPLA while pathways regulating cellular responses to stimuli and stress
291 were downregulated with CAF01 (**Figure 3E**). Collectively, transcriptional profiles demonstrated

292 activation of effector programs within CD4 T cells with common and unique pathways induced
293 across vaccine platforms.
294
295 Consistent with this, $CD95^+$ CD4 T cells at P1w2 and P2w3 exhibited notable clustering patterns
296 across vaccine regimens. Particularly, tighter, and more distinct clusters were observed at P1w2
297 compared to P2w3 notably with CAF01 (**Figures 3F, Supplementary Figure 4D-E**). Exploration
298 of genes regulating T_h1 and T_h17 programs within CD95+ CD4 T cells at P1w2 showed that
299 CD95+ CD4 T cells in both MPLA and CAF01 groups exhibited overlapping expression profiles,
300 with genes regulating major classes of cytokine-cytokine receptor interactions represented. The
301 MPLA group exhibited higher expression levels of IFN-induced chemokines CXCL10 and
302 CXCL11, IL1 family members IL18 and IL1RAP, IL15 family members IL15 and IL15RA, as well
303 as TNF cytokine family members FAS, TNFα, TNFRSF8 (CD30), and TNFRSF9 (4-1BB)
304 (**Figure 3G-H, Supplementary Figure 4F**).
305
306 In contrast, the CAF01 group demonstrated expression of the T_h17 receptor IL23R, along with
307 TNF family members FASLG, TNFRSF13B (TACI), TNFRSF11 (RANKL), and TNFRSF12
308 (DR3) within CD95+ cells with higher relative expression of IL17A observed with CAF01,
309 indicative of T_h17 responses (**Figure 3I, Supplementary Figure 4G**). Collectively, this gene-
310 level analysis indicated strong engagement of T_h1 molecular programs within LN CD4 T cells
311 with MPLA.
312
313 **Phenotypically and functionally specialized GC $T_{fh}1$ / $T_{fh}17$ subsets elicited with HIV-1**
314 **Env Formulated in CAF01 and MPLA+QS-21 Adjuvants.**
315 After confirming the robust induction of GC responses by both vaccines and observing distinct
316 molecular programs in CD4 T cells, we proceeded to investigate the phenotypic and functional
317 characteristics of T_{fh} cells. We examined the GC T_{fh} cell subset characterized by the expression

318 of CXCR5 and high levels of PD-1, using the gating strategy outlined in **Supplementary Figure**
319 **5A.** Our analysis of the lymph nodes revealed an increase in the frequencies of GC T_{fh} cells
320 following each protein boost in both groups compared to baseline. Importantly, there were no
321 statistically significant differences observed between the two adjuvant platforms, as shown in
322 **Figure 4A**. We further examined the frequencies of T_{fh} cells characterized by the expression of
323 CXCR5 and PD-1 (CXCR5+ PD-1+), which also exhibited a significant increase following the first
324 protein boost in both groups (**Supplementary Figure 5B**).
325
326 To gain insights into the T_{fh} helper profiles within the GC, we assessed the expression of CXCR3
327 ($T_{fh}1$) and CCR6 ($T_{fh}17$) on the GC T_{fh} cells. Both adjuvants induced GC $T_{fh}1$ cells, as evidenced
328 by the expression of CXCR3. However, a selective increase in GC $T_{fh}1/17$ cells was observed
329 with CAF01, as shown in **Figure 4B**. While the frequencies of GC $T_{fh}17$ cells did not show a
330 significant increase following immunization, Boolean analysis revealed a higher relative
331 proportion of this subset with CAF01, along with a corresponding higher proportion of GC $T_{fh}1$
332 subset with MPLA at P1w2, as demonstrated in **Figure 4C.**
333
334 Following the observed induction of LN $T_{fh}1$ responses, we quantified the Env-specific CD4 T cell
335 response using intracellular cytokine staining (ICS). The analysis revealed higher relative
336 frequencies of Env-specific T_{fh} cells and Env-specific CXCR5- CD4 T cells producing IFNγ with
337 MPLA compared to CAF01 **(Supplementary Figure 5C**). To obtain a more comprehensive
338 understanding of the cytokine profile within the LN $T_{fh}1$ and $T_{fh}17$ subsets, we assessed cytokine
339 production after PMA/Ionomycin stimulation (**Figure 4D**). By utilizing the discrete expression
340 patterns of CXCR3 and CCR6 on CXCR5+ CD4 T cells in the LN, in conjunction with the canonical
341 cytokines IFNγ (T_h1), IL-17 (T_h17), and IL-21 (T_{fh}), we made several important observations.
342 Firstly, we found that within the $T_{fh}1$ subset, IL-21+ IFNγ+ co-producing cells were more abundant,
343 and their levels were significantly increased with MPLA stimulation (**Figure 4E**). Conversely,

344 within the $T_{fh}17$ subset, we observed that IL-21+ IL-17+ co-producing cells were more abundant,
345 and their levels were significantly higher in the CAF01 group. Notably, the $T_{fh}1/17$ subset
346 demonstrated the highest degree of polyfunctionality, as evidenced by the production of multiple
347 cytokines.
348
349 We further analyzed the cytokine profiles by gating IFNγ and IL-21 co-producers versus IL-21
350 single producers. This analysis revealed that both subsets, $T_{fh}1$ and $T_{fh}17$, produced IL-2 and
351 TNFα. However, IL-17 production was predominantly observed in IFNγ-negative, IL-21+ cells
352 (**Supplementary Figure 5D**). To assess systemic levels of IL-21, we measured serum IL-21. We
353 found a significant induction of IL-21 in both vaccine groups at day 7 post-immunization, with no
354 observable differences observed across the adjuvant platforms (**Supplementary Figure 5E**).
355 This suggests that the induction of IL-21 is a common feature of both vaccine formulations.
356 Overall, these findings suggest that MPLA preferentially induces the production of IL-21+ IFNγ+
357 cells within the $T_{fh}1$ subset, while CAF01 promotes the generation of IL-21+ IL-17+ cells within
358 the $T_{fh}17$ subset. Furthermore, the $T_{fh}1/17$ subset exhibits the most diverse cytokine production
359 profile among the subsets examined.
360
361 To investigate whether the effects of MPLA versus CAF01 adjuvants were also evident in
362 circulating T_{fh} counterparts, we assessed pT_{fh} responses. We observed a significant increase in
363 proliferating pT_{fh} cells, with a predominant induction of $pT_{fh}1$ cells similar to the phenotype
364 observed in the LN, when MPLA was used as the adjuvant (**Figure 4F**). In contrast, no evidence
365 of a $T_{fh}17$ or $T_{fh}1/17$ bias in pT_{fh} cells was observed with CAF01 (data not shown).
366 To evaluate Env-specific T_{fh} cell abundance, we utilized the AIM assay (**Supplementary Figure**
367 **5F**). The analysis showed a higher relative induction of Env-specific T_{fh} responses with MPLA at
368 P1w1 but not P2w1 (**Figure 4G**), which was further corroborated by ICS assays (**Figure 4H**). The
369 frequencies of CXCR5+ cells co-producing IL-2 and IFNγ, as well as cells co-producing IL-21 and

370 IFNγ, indicated that higher numbers of IFNγ+ Env-specific pT_{fh} cells were induced with MPLA at
371 P1w1 and P2w1 (**Figure 4I**). Therefore, formulation of gp140 with MPLA induced strong T_h1-
372 polarized GC T_{fh} responses, characterized by a higher magnitude of IFNγ+ anti-Env T_{fh} cells.
373
374 **Induction of persistent anti-Env IgG antibodies with HIV-1 Env/MPLA+QS-21.**
375 We next sought to determine whether induction of higher frequencies of Env-specific $T_{fh}1$ cells
376 with MPLA could effectively enhance B cell proliferation and differentiation, in turn, promoting the
377 development of Env antibodies with heightened affinity and increased durability. To this end, we
378 performed a wide repertoire of quantitative and functional assays to assess the magnitude,
379 durability, affinity, avidity, breadth, and effector functionality of vaccine induced humoral
380 responses to Env. Longitudinal measures of binding antibody concentrations in sera against
381 C.1086 Env showed rapid and equivalent recall in all animals post P1, with antibodies reaching
382 peak levels after the 2nd protein boost. While antibody kinetics were comparable across vaccine
383 groups, significantly higher antibody magnitude was elicited by MPLA at week 8 post 2nd boost
384 and until 30 weeks after final immunization (**Figure 5A**). At this protracted memory time point,
385 serum antibody concentrations were, on average, 2.5-fold higher with MPLA (median [ng/ml];
386 MPLA, 5566 versus CAF01, 2155) (**Figure 5B**). To assess CD4 correlates of antibody durability,
387 we asked whether the magnitude of vaccine-elicited GC T_{fh} subsets after each boost predicted
388 antibody concentrations at week 30. Two key cellular determinants of antibody durability emerged
389 from our analysis: GC $T_{fh}1$ cell magnitude ($p < 0.05$, $r=0.65$) (**Figure 5C**) and frequencies of IFNγ+
390 IL-2+ Env-specific LN T_{fh} cells ($p < 0.05$, $r = 0.62$) (**Figure 5D**). These data in concert with IFNγ-
391 regulated molecular programs induced in LN CD4 T cells support a role for GC $T_{fh}1$ induction in
392 antibody persistence.
393 Using a binding antibody multiplex assay (BAMA), we further confirmed that stronger memory
394 responses were elicited by MPLA evidenced by higher median serum IgG antibody concentrations
395 to C.1086 gp140 and gp120 antigens measured as area-under-the curve (AUC) over time (**Figure**

396 **5E-F**). Thus, utilizing two orthogonal approaches, the data showed significantly higher and
397 protracted serum antibody responses against autologous Env with MPLA, indicative of efficient
398 T_{fh} cell mediated B cell recruitment into the long-lived plasma cell pool.
399
400 We next sought to understand if $T_{fh}1$ profile was also associated with improved Env antibody
401 breadth. Therefore, we tested serum reactivity against an antigen panel comprising of consensus
402 gp140 proteins and found that antibodies with higher cross-clade reactivity were induced with
403 MPLA relative to CAF01 (**Figure 5G-H**). We extended these analyses to assess reactivity to V1V2
404 loops of 1086C and noted that antibodies with significantly higher specificity to these important
405 regions within Env were induced in both vaccine regimens (**Figure 5I**).
406
407 Having established induction of robust serum Env antibodies with MPLA, we next determined
408 whether Env-specific IgG reactivity would also be higher within rectal secretions. After
409 normalization for total IgG levels within rectal secretions, the data showed that Env antibodies
410 were effectively recalled in most animals at week 2 post 2nd protein boost and persisted in all
411 animals 8 weeks after final immunization. However, akin to the systemic compartment, gp140 IgG
412 in rectal secretions were significantly higher with MPLA at memory time point (**Figure 5J**), with 6-
413 fold higher levels in MPLA relative to CAF01 at week 8 after final immunization (**Figure 5K**). In
414 both vaccine regimens, the induction of Env-IgA antibodies was poor, preventing a quantitative
415 assessment of IgA responses in secretions.
416
417 **Induction of IgG1 subclass antibodies with greater effector functions with HIV-1**
418 **Env/MPLA+QS-21.**
419 Since antibody effector functions, facilitated by interaction of Ig constant region with cognate Fc
420 receptors on innate cells, mediate protection from acquisition and viral control (Carpenter and
421 Ackerman 2020), we assessed the IgG subclass profile at week 2 post 2nd protein boost. Both

422 CAF01 and MPLA+QS-21 induced Env-specific IgG1, and modest levels of IgG2, and IgG4
423 isotypes with higher IgG1 in all animals, with exception of one animal with higher IgG4 (**S6**).
424
425 Significantly higher IgG1 was induced by MPLA relative to CAF01 (**Figure 6A**), while IgG2 and
426 IgG4 antibody subclasses were comparably induced (**Figure 6B-C**). The improved IgG1 subtype
427 antibody responses with MPLA prompted us to determine whether a corresponding increase in
428 antibody effector functions might also be observed. Measurement of antibody-dependent
429 phagocytosis (ADP) suggested enhanced effector functions with MPLA (**Figure 6D-E**) which
430 strongly correlated with Env IgG1 but not IgG2 or IgG4 (**Figure 6F**).
431
432 Finally, we observed higher levels of neutralizing antibodies against the tier 1A MW965.26 at peak
433 (2 weeks post 2nd protein boost) with MPLA relative to the CAF01 platform (**Figure 6G**). Antibody
434 avidity measurements revealed relatively higher avidity with MPLA against autologous Env
435 including V1V2 loops and to consensus Env proteins (**Figure 6H-L**). Collectively, these findings
436 provide compelling evidence for significantly increased antibody quality associated with induction
437 of GC T_{fh}1 cells.
438
439 **Differentiation of GC T_{fh} Subsets initiated during the DNA Priming Phase.**
440 Finally, we sought to determine the degree to which T_{fh} responses elicited during the priming
441 phase influenced antibody responses post 1st protein boost. To this end, we analyzed blood
442 samples at weeks 0, 1, 2, and 4, while also evaluating FNA of the draining LN at week 2 after the
443 3rd DNA prime (**Figure 7A**).
444
445 Animals were immunized with C.1086 DNA expressing IP10 (DNA_{IP10}) which primes stronger GC
446 T_{fh} responses relative to DNA-alone (Verma, Schmidt et al. 2019). To further enhance GC T_{fh}
447 responses, beyond that induced by DNA_{IP10}, we engineered DNA_{IP10} to co-express IL-6, a key

448 cytokine promoting T_{fh} differentiation. Our vector achieved coordinate expression of Gag and Env
449 antigens together with IP10+IL6 as confirmed in transfected 293T cells (**Figure 7B**). Following
450 three rounds of intradermal immunization with DNA_{IP10} or $DNA_{IP10+IL6}$, we assessed proliferating
451 pT_{fh} cells (Ki-67^{+} PD-1^{+} of CXCR5+ CD4 T cells in blood, **7C**). We observed a significant increase
452 at weeks 1 and 2 with $DNA_{IP10+IL6}$ but not DNA_{IP10} indicating that IP10+IL6 incorporation promoted
453 T_{fh} differentiation. Additionally, T_{fh} induction was accompanied by notable $T_{fh}1$ skewing within
454 proliferating pT_{fh} cells (median $pT_{fh}1$ at day 0 (% CD95), 0.89% versus 1.48% at day 7 and 14).
455 Measurement of antigen-specific responses by AIM assay demonstrated induction of Env and
456 Gag-specific pT_{fh} cells with a trend for higher responses elicited by $DNA_{IP10+IL6}$ (median, 0.42%,
457 IQR 0.3- 1.7%) relative to D_{IP10} (median, 0.12%; IQR: 0.04 – 1.4%, **Supplementary Figure 7**).
458
459 Based on the transient accumulation of pT_{fh} cells in the blood, we further explored GC T_{fh}
460 responses. Out of twelve collected FNAs, eight were successful (four per vaccine group), and
461 demonstrated significant increase in GC T_{fh} frequencies following vaccination (**Figure 7D**). Gating
462 on Ki-67+ cells encompassing both CXCR5+ PD-1+ and PD-1++ subsets, an increase in activated
463 T_{fh} cells within the LN was observed (**Figure 7E**), accompanied by a corresponding increase in
464 the $T_{fh}1$ subset (**Figure 7F**). Altogether, these data demonstrate induction of GC $T_{fh}1$ responses
465 during the priming phase post immunization with DNA_{IP10} or $DNA_{IP10+IL6}$.
466
467 Measurement of C.1086 Env antibodies in serum revealed induction of antibody responses after
468 the 3rd prime in 8/12 animals, with comparable kinetics across vaccine groups. Notably, antibody
469 concentrations 4 weeks post 3rd DNA prime strongly correlated with both the frequencies of
470 proliferating T_{fh} cells (Ki-67+ PD-1+ CXCR5+) within the LN and with the proliferating $T_{fh}1$ (Ki-67+
471 PD-1+ CXCR5+ CXCR3+) subset at 2 weeks post 3rd DNA prime (**Figure 7G-H)**. Moreover, the
472 strong association of antibody concentrations after the 3rd DNA prime with peak antibodies
473 following the 1st protein boost (**Figure 7I**) indicated efficient recall of Env-specific memory B cells

474 induced during the prime. Overall, the data show that stimulation of $T_{fh}1$ cells during the DNA
475 priming stage is closely linked with robust antibodies post boost.
476
477 In summary, our results strongly support maximizing GC $T_{fh}1$ responses during both the prime
478 and boost phases as a strategy to generate potent and durable humoral immunity. These findings
479 have significant implications for the development of more effective vaccination strategies aimed
480 at eliciting robust and long-lasting immune responses.
481
482
483
484
485
486
487
488
489
490
491
492
493
494
495
496
497
498
499
500
501
502
503
504
505
506
507
508
509
510
511
512
513
514

515 **DISCUSSION**

516 T_{fh} cells are fundamental in establishing long-lasting humoral immunity with vaccination. The
517 dynamic interplay between innate immune activation and the ensuing inflammatory response
518 directs the magnitude and composition of T_{fh} cell populations, ultimately shaping quantitative and
519 qualitative features of humoral memory (Hirota, Turner et al. 2013, Barbet, Sander et al. 2018,
520 Olatunde, Hale et al. 2021). Here we show that maximizing induction of CXCR3+ $T_{fh}1$ cells
521 correlates with serum Env antibodies which exhibit higher persistence. Our studies with LAMV
522 revealed the robust induction of $pT_{fh}1$ and GC $T_{fh}1$ responses, along with a moderate induction of
523 $T_{fh}17$ and $T_{fh}1/17$ cells. These findings led us to compare the adjuvants MPLA+QS-21 and CAF01,
524 known to elicit T_h1 and mixed $T_h1/17$ responses (Christensen, Bollehuus Hansen et al. 2019),
525 (Pedersen, Andersen et al. 2018) respectively, to determine the optimal strategy for maximizing
526 Env antibody persistence. Through proteomic and transcriptomic analysis of lymph nodes, we
527 uncovered evidence of robust GC responses induced by both vaccine adjuvants following a DNA
528 prime. Moreover, we observed notable skewing of T_{fh} responses, which corresponded with the
529 elicitation of distinct immunogenicity profiles. Interesting, although peak antibody responses
530 following each protein boost were similar across the vaccine platforms, our investigation revealed
531 a notable distinction in antibody persistence. Specifically, the MPLA+QS-21 regimen exhibited
532 higher antibody levels at week 8,12, and 30, suggestive of enhanced support from T_{fh} cells in
533 promoting plasma cell differentiation. Moreover, $T_{fh}1$ cell induction during the DNA priming phase
534 was linked to effective boosting upon subsequent protein immunization. These findings highlight
535 the critical role of $T_{fh}1$ cells in driving the longevity of antibody responses and emphasize the
536 potential of stimulating $T_{fh}1$ cells during the prime and boost to elicit durable humoral immunity
537 against HIV Env.

538

539 A significant finding in RV144 vaccine recipients was the correlation between Env-specific
540 peripheral CD4 T cell subsets co-producing IFNγ, TNFα, CD40L, and IL4, and a reduced risk of

541 HIV acquisition [40]. This correlation suggests that productive GC responses elicited by the
542 vaccine fostered protective humoral immunity (Lin, Finak et al. 2015). More recently, follow up
543 analysis of this population in n=6 subjects immunized with the RV144 vaccine regimen in South
544 Africa (HVTN 097) reported a pT_h2 biased transcriptional profile based on observed IL4 and IL13
545 transcripts (Cohen, Tian et al. 2022). However, it is important to note that in addition to T_h2 cells
546 CD4 T_{fh} cells also produce IL-4 in a SLAM/SAP dependent manner (McCausland, Yusuf et al.
547 2007) and T_h1 cells can produce IL-13 in the presence of IL18 is documented (Hayashi,
548 Yoshimoto et al. 2007). These findings indicate the need for utilizing multiple immune parameters
549 when categorizing CD4 T cell help and underscore the importance of studying both lymph node
550 and peripheral blood CD4 T_{fh} cells to fully understand their respective roles in fostering Env
551 antibody responses.
552
553 In the context of vaccination, our observed association between T_{fh}1 cells and persistent antibody
554 responses raises the possibly that higher relative production of IL-21 and CD40L may support the
555 proliferation of GC B cells in concert with IFNγ-mediated B cell proliferation. This contention is
556 supported by the observation of higher relative Ki-67 protein levels in the MPLA group at week 2
557 of the first protein boost. In the context of a T_h1 driven GC response rich in CXCL chemokines
558 CXCL9, 10, and 11; CXCR3 expression on T_{fh} cells may furthermore enable proximity and
559 interaction with GC B cells. CAF01 is composed of cationic liposomal vesicle
560 (dimethyldioctadecylammonium, DDA) together with a synthetic analog of a mycobacterial cell
561 wall (trehalose dibehenate, TDB), a potent activator of macrophages and dendritic cells through
562 the macrophage inducible $Ca2^+$-dependent lectin receptor Mincle, a pattern recognition receptor
563 recognizing bacterial lipids (Davidsen, Rosenkrands et al. 2005, Martinez-Lopez, Iborra et al.
564 2019). CAF01 elicits CD4 T_h1 responses while concurrently driving strong T_h17 responses to a
565 mycobacterium TB subunit vaccine via induction of proinflammatory cytokines IL-1β, IL-6, and
566 TNF-α (Werninghaus, Babiak et al. 2009). We observed that CAF01 was effective in inducing

567 robust cellular responses, which were skewed towards a T_h1/T_h17 profile within GCs. It is possible
568 that employing the CAF06 platform which incorporates MPL into the bilayer of DDA/TDB
569 liposomes may drive stronger T_h1 responses together with T_h17 cells thereby enhancing
570 protective immunity by eliciting strong humoral immune responses.
571
572 The present studies are the first to our knowledge to assess immunological responses across HIV
573 vaccine platforms with MPLA and CAF01-based adjuvants and strongly support GC $T_{fh}1$ cell
574 induction for enhancing Env antibody responses. However, our study has several limitations. First,
575 priming modalities across MPLA and CAF01 were not identical. Animals boosted with MPLA were
576 primed with DNA_{IP10}, whereas CAF01 boosted animals received the $DNA_{IP10+IL6}$ prime. Given the
577 stronger immunogenicity of $DNA_{IP10+IL6}$, it is possible that our studies underestimate immune recall
578 potential of MPLA relative to CAF01. Second, 5/6 animals in each vaccine group were males and
579 therefore our findings do not capture possible variability in vaccine response between sexes.
580 Because females develop higher antibody responses than males, it is important to test our
581 hypothesis in animals of both sexes(Fischinger, Boudreau et al. 2019). Third, the interplay of
582 innate immune cells and the follicular dendritic cell network in regulation of T_{fh} help for antibody
583 responses is an important consideration for future studies. Finally, we did not assess vaccine
584 efficacy and therefore whether GC $T_{fh}1$ cells constitute an important correlate of protection from
585 acquisition remains an important unanswered question.
586
587 In summary, our findings demonstrate significant skewing of the GC T_{fh} response by adjuvants
588 inducing distinct inflammatory responses. We further demonstrate that induction of $T_{fh}1$ cells
589 results in superior persistence of Env antibodies indicating that strategies to harness this CD4
590 subset may promote protective humoral immunity against HIV.
591
592

593 **MATERIALS AND METHODS**

594 **Table 1: Flow Cytometry Antibodies**

Antibody name	Panel	Vendor	Catalog number/Identifier
Mouse anti-human CD3 (Clone SP34-2)	T_{FH}/AIM/ICS	BD Biosciences	Cat#557917; RRID: AB_396938
Mouse anti-human CD4 (Clone L200)	T_{FH}/AIM/ICS	BD Biosciences	Cat#563737; RRID: AB2687486
Mouse anti-human CD8 (Clone SK-1)	T_{FH}/AIM/ICS	BD Biosciences	Cat#564913; RRID: AB_2833078
Mouse anti-human CD14 (Clone MSE2)	T_{FH} Panel	BioLegend	Cat#301822; RRID: AB_493747
Mouse anti-human CD16 (Clone 3G8)	T_{FH} Panel	BD Biosciences	Cat#563172; RRID: AB_2744297
Mouse anti-human CD20 (Clone 2H7)	T_{FH} Panel	BioLegend	Cat#302314; RRID: AB_314262
Mouse anti-human CD69 (Clone FN50)	T_{FH} Panel	BioLegend	Cat#310944; RRID: AB_2566466
Mouse anti-human CD95 (Clone DX2)	T_{FH}/AIM/ICS	BioLegend	Cat#564710; RRID: AB_2738907
Mouse anti-human CXCR3 (CD183) (Clone 1C6)	T_{FH} Panel	BD Biosciences	Cat# 550967; RRID: AB_398481
Mouse anti-human CXCR5 (CD185) (Clone MU5UBEE)	T_{FH}/AIM/ICS	eBioscience	Cat#12-9185-42; RRID: AB_11219877
Mouse anti-human CCR6 (CD196) (Clone G034E3)	T_{FH} Panel	BioLegend	Cat#353430; RRID: AB_2564233
Armenian Hamster anti- ICOS (CD278) (Clone C396.4A)	T_{FH} Panel	BioLegend	Cat#313534; RRID: AB_2629729
PECy7 anti-human PD1 (CD279) (Clone EH12.2H8)	T_{FH} Panel	BioLegend	Cat# 329918, RRID: AB_2159324
Mouse anti-human Bcl-6 (Clone K112-91)	T_{FH} Panel	BD Biosciences	Cat# 563581
Mouse anti-Ki-67 (Clone B56)	T_{FH} Panel	BD Biosciences	Cat#558616; RRID: AB_10611866
Mouse anti-human CD25 (Clone BC96)	AIM assay	eBioscience	Cat#**53-0259-42** RRID: AB_2043827
Mouse anti-human CD134 (OX-40) (Clone L106)	AIM assay	BD Biosciences	Cat#744746; RRID: AB_2742454
Mouse anti-human CD137 (4-1BB) (Clone 4B4-1)	AIM assay	BioLegend	Cat# 309826; RRID: AB_2566260
Mouse anti-human CD154 (CD40L) (Clone 24-31)	AIM assay	eBioscience	Cat#17154842 RRID:AB_1582215
Mouse anti-human TNF-α (Clone Mab11)	ICS assay	BioLegend	Cat# 502906; RRID: AB_315258
Mouse anti-human IFNγ (Clone B27)	ICS assay	BioLegend	Cat# 506518; RRID: AB_2123321
Mouse anti-human IL2 (Clone MO1-17H12)	ICS assay	BioLegend	Cat# 500344; RRID: AB_2564091

Mouse anti-human IL-17 (Clone eBio64DEC17)	ICS assay	eBioscience	Cat# 48-7179-42; RRID: AB_10853643
Mouse anti-human IL-21 (Clone 3A3-N2.1)	ICS assay	BD Biosciences	Cat# 560493; RRID: AB_1645421
APC-Cy7 live/dead		Life Technologies	Cat#L34976
BV510 live/dead		Life Technologies	Cat#L34966

Table 2. Samples for RNA seq and Spatial profiling

S.No	**Animals ID**	**Vaccine group**	**Lymph node collection time points and cells used for**		
			Baseline (WK0)	**Week2 post 1st protein boost**	**Week3 post 2nd protein boost**
1	**47161**	MPLA+QS-21	RNA seq	RNA seq	RNA seq
2	**45781**	MPLA+QS-21	Spatial profiling	Spatial profiling	Spatial profiling
3	**46235**	MPLA+QS-21	Spatial profiling	Spatial profiling	Spatial profiling
4	**46551**	MPLA+QS-21	Spatial profiling	Spatial profiling	Spatial profiling
5	**46548**	MPLA+QS-21	RNA seq	RNA seq	RNA seq
6	**47081**	MPLA+QS-21	RNA seq	RNA seq	RNA seq
7	**45721**	CAF01	RNA seq+Spatial profiling	RNA seq+Spatial profiling	RNA seq+Spatial profiling
8	**47154**	CAF01	NA	NA	NA
9	**46410**	CAF01	Spatial profiling	Spatial profiling	Spatial profiling
10	**46354**	CAF01	RNA seq	RNA seq	RNA seq
11	**47466**	CAF01	RNA seq	RNA seq	RNA seq
12	**47387**	CAF01	Spatial profiling	Spatial profiling	Spatial profiling

Rhesus Macaques. For LAMV studies, sixteen female colony-bred rhesus Indian origin rhesus macaques (*Macaca mulatta*) were utilized. Animals were dichotomized by age into two groups; young [n=8, mean=4 years] and aged [n=8, mean=16 years]. Young adults with a higher baseline weight [mean=5.9kg] were selected for the cohort to closer match the aged animals in size [mean=8.6kg]. For the HIV vaccine study, twelve adult (10 males and 2 females) Indian origin rhesus macaques (*Macaca mulatta*) were utilized. At study initiation, animals were 3.4 – 5.6 years of age with a median weight of 6.8 kg. Animals in both studies were SIV negative (SIV-), simian T-cell leukemia virus negative (STLV-), and simian retrovirus negative (SRV-); and had no history of dietary, pharmacological, or surgical manipulation (*Supplementary Table 1a*). All animals were

607 bred and housed at the California National Primate Research Center (CNPRC) in accordance
608 with the American Association for Accreditation of Laboratory Animal Care (AAALAC) guidelines.
609 All studies were approved by the University of California, Davis Institutional Animal Care and Use
610 Committee (IACUC).
611
612 **LAMV Immunization.** The animals received an IM booster vaccination of canine distemper-
613 measles vaccine (Vanguard).
614
615 **HIV-1 Immunization.** Animals were immunized with DNA vaccines intradermally in both thighs at
616 weeks 0, 4, and 8. At each prime, animals received 4mg of the pGA2/JS2 plasmid DNA encoding
617 either SHIV C.1086 T/F Env + rhesus interferon-induced protein (IP)-10 (Group 1; n=6) or SHIV
618 C.1086 T/F Env + rhesus interferon-induced protein (IP)-10 + rhesus interleukin (IL)-6 (Group 2;
619 n=6). Subsequent protein boosters were administered at weeks 12 and 20 with Group 1 animals
620 receiving 50μg C.ZA 1197MB gp140 protein adjuvanted with MPLA + QS-21 and Group 2 animals
621 receiving 50μg C.ZA 1197MB gp140 protein adjuvanted with CAF01 delivered in a 175μL volume
622 subcutaneously into each thigh.
623
624 **Cationic Adjuvant Formulation 01 (CAF01).** CAF01 was generously provided by Statens Serum
625 Institut, Denmark. Admixing with protein was performed by addition of 25μg of C.ZA 1197MB
626 gp140 protein (Immune Technology, USA) to 250μL of CAF01 (625μg DDA+ 125μg TDB)
627 adjuvant formulation. The solution was vortexed vigorously for 15-30 seconds followed by visual
628 inspection. Remaining protein was added in 10μg increments with intermittent vortexing until a
629 final amount of 100μg gp140 was achieved.
630

631 **Monophosphoryl Lipid A (MPLA).** Synthetic MPLA was purchased from InvivoGen, USA. 100μg
632 C.ZA 1197MB gp140 protein was dissolved in a solution of 100μg MPLA with 50μg QS-21 saponin
633 [Desert King International, USA] (2:2:1) in PBS.
634
635 **Specimen collection and processing.** Lymph node (LN) biopsies were obtained at baseline
636 (week0), week 14 (week 2 post 1st protein boost) and week 23 (week 3 post 2nd protein boost)
637 and processed as described previously(Verma, Schmidt et al. 2019). Isolated cells were washed
638 in complete media, counted, and cryopreserved until subsequent analysis. Two weeks after the
639 3rd DNA immunization, fine needle aspirates of LN were obtained using a 22-gauge needle, as
640 previously described(Verma, Schmidt et al. 2019). PBMCs were isolated from whole blood
641 collected in CPT vacutainer tubes at weeks 0, 4, 9, 10, 13, 21, and 32 . Serum was collected from
642 animals at weeks 0, 4, 8, 8+day3, 9,10, 12, 13, 14, 16, 20, 20+day3, 21, 22, 23, 28, 32, 50
643 timepoints and stored at -80°C until subsequent analysis. Rectal secretions were collected for
644 assessment of mucosal antibody production using premoistened Weck-Cel sponges as
645 previously described(Verma, Schmidt et al. 2019).
646
647 **Activation induced Marker and Intracellular cytokine staining assay.** Detection of antigen
648 specific CD4 T cells detection was quantified by Activation induced Marker (AIM) and intracellular
649 cytokine staining (ICS). PBMCs/LN cells were stimulated with overlapping peptide pools of HIV
650 consensus C and HIV-1 C.1086 Env gp140C protein (NIH AIDS Reagent Program) in AIM/R10
651 media in the presence of 0.2μg CD28/49d co-stimulatory antibodies (BD) per test. As a positive
652 control, cells were stimulated with 1X Cell Stimulation Cocktail (PMA and ionomycin)
653 (eBioscience, USA). Unstimulated controls were treated with volume-controlled DMSO (Sigma-
654 Aldrich). Tubes were incubated in 5% CO_2 at 37°C overnight for AIM assay. For ICS assay, after
655 1 hour of stimulations, protein transport inhibitors 2μl/mL GolgiPlug (Brefeldin A) and 1.3μl/mL

656 GolgiStop (Monensin) (BD, Biosciences, USA) were added to the tubes for 8 hours at 37°C, 5%
657 CO_2. Following stimulation, the cells were stained for AIM and ICS surface markers (see the Table
658 1). Cells were then fixed with cytofix/cytoperm for 10 min at 4°C, permeabilized with 1X Perm
659 wash buffer (BD, Biosciences, USA), and stained with intracellular markers (see the Table 1) for
660 45 min. Cells were then washed and acquired the same day on a BD FACSymohony.
661
662 **T_{fh} cell staining by flow cytometry and cell sorting.** T_{fh} cell staining was performed on whole
663 blood and LN cells as previously described(Verma, Schmidt et al. 2019). Samples were acquired
664 on BD FACSymphony with FACS Diva version 8.0.1 software and data were analyzed using
665 FlowJo (Versions 9 and 10). For cell sorting, cryopreserved cells were enriched by NHP CD4
666 isolation kit (Miltenyi Biotec,USA) and cells stained with CD3, CD4, CXCR5, CD95, and live/dead
667 in complete media (incubated for 1 hour at 4°C on a shaker). Stained cells were washed twice
668 with 5mL RPMI plain media (Gibco, USA) and cell pellets were resuspended in 0.5mL sorting
669 buffer containing 2% FBS+PBS. The cells were then filtered through a 40μM strainer into 5mL
670 sterile FACS tube (Blue cap tube). Cell sorting was performed using a BD FACSAria III. Naive,
671 and CD95+ CD4 T cell populations were collected in complete media supplemented with 20%
672 FBS. Sorted cells were stimulated with overlapping peptide pools of HIV consensus C and HIV-1
673 C.1086 Env gp140C protein (NIH AIDS Reagent Program) in R10 media in the presence of
674 0.2μg/mL CD28/49d co-stimulatory antibodies (BD) for 14 hours. The culture supernatant and
675 stimulated cells were collected and stored at -80°C for subsequent analysis.
676
677 **Serum IL-21 ELISA.** Serum IL-21 cytokine was quantified using an IL-21 ELISA Development kit
678 (Novus Bio, USA) in accordance with manufacturer's protocol. Briefly, the capture mAb (MT216G)
679 diluted to 2μg/mL in PBS, pH 7.4 was added (100μL/well) to 96-well microtiter plates with high
680 binding capacity (Thermo Fisher, USA) and incubated overnight at 4°C. The next day, plates were

681 aspirated, and wells blocked with 200μL/well of PBS with 0.05% Tween 20 and 0.1% BSA
682 (incubation buffer). After 1 hour of incubation, plates were washed 5 times with PBS containing
683 0.05% Tween 20 (300μL/well). Samples or working standards were added at 100uL/well and
684 incubated for 2 hours at room temperature. After washing, plates were incubated for one hour
685 with 100μL/well of detection mAb diluted to 1μg/mL in incubation buffer. Streptavidin-HRP diluted
686 1: 1000 in incubation buffer was added to the plates at 100uL/well for 1 hour followed by washing.
687 Plates were washed and then developed with TMB substrate (Thermo Fisher, USA), and the
688 reaction quenched with 0.2M H_2SO_4 (Sigma, USA). Absorbance was recorded using a
689 Spectramax 5 plate reader (Molecular Devices) at 450 nm with a reference filter at 570 nm within
690 15 min. The concentration of IL-21 in serum was calculated based on an IL-21 standard curve
691 using SoftMax Pro.
692
693 **RNA Sequencing and Bioinformatics.** RNA was extracted from sorted naive, and CD95+ CD4
694 T cells using a RNeasy plus mini kit (QIAgen). Isolated RNA sample quality was assessed using
695 BioAnalyzer RNA pico assay (Agilent Technologies Inc., California, USA) and quantified by Qubit
696 2.0 RNA HS assay (ThermoFisher, Massachusetts, USA). Library construction was performed
697 based on manufacturer's recommendation for SMART-Seq® v4 Ultra® Low Input RNA Kit
698 (Takara Bio USA Inc., California, USA) followed by Nextera® XT DNA Library Prep Kit (Illumina,
699 California, USA). Final library quantity was measured by KAPA SYBR® FAST qPCR and library
700 quality evaluated by TapeStation D1000 ScreenTape (Agilent Technologies, CA, USA). Final
701 library size was about 450bp with an insert size of about 300bp. Illumina® 8-nt dual-indices were
702 used. Equimolar pooling of libraries was performed based on QC values and sequenced on an
703 Illumina® NovaSeq S4 (Illumina, California, USA) with a read length configuration of 150 PE for
704 40 M PE reads per sample (20M in each direction). Reference rhesus macaque genome
705 (*Macaca_mulatta* _GCF_003339765.1_Mmul_10) and gene model annotation files were
706 downloaded from genome website directly. Index of the reference genome was built using Hisat2

707 v2.0.5 and paired-end clean reads were aligned to the reference genome using Hisat2 v2.0.5.
708 The mapped reads of each sample were assembled by StringTie (v1.3.3b) in a reference-based
709 approach.
710 The quality of the raw RNA-seq data was assessed using FastQC, and poor-quality ends were
711 trimmed (Trimgalore). High-quality sequences were aligned against the Macaca mulatta
712 reference genome using STAR aligner v2.7.9, and counts were generated using featureCount
713 (Dobin, Davis et al. 2013). A list of differentially expressed genes (DEGs) were generated using
714 DESeq2 based on the negative binomial distribution(Love, Huber et al. 2014). The resulting DEGs
715 between the groups were defined at cut-off criteria of $|\log_2 \text{fold-change}| \geq 1.5$ and p-value < 0.05
716 adjusted using the Benjamini and Hochberg's approach for controlling the false discovery rate
717 (Liao, Smyth et al. 2013). Gene set enrichment analysis (Subramanian, Tamayo et al. 2005) was
718 used to assess the statistical enrichment of gene ontologies, and pathways, and visualized using
719 Clusterprofiler v4.8.1(2012). All statistical analyses were performed using R 4.2.0.
720
721 **GeoMx Digital Spatial Profiling (DSP).** Formalin-fixed paraffin-embedded (FFPE) blocks were
722 prepared using lymph node tissue from biopsies at baseline, week2 post protein1, and week3
723 post protein2 immunization timepoints to analyze the spatial protein profiling using the Nanostring
724 GeoMx Digital Spatial Profiler (DSP). The tissue sections of 5-µm thickness were cut from FFPE
725 blocks and mounted on GeoMx-NGS BOND RX slide as per manufacturer's recommendations.
726 Sections were baked at 60°C for 30 minutes, deparaffinized, rehydrated in CitriSolv, ethanol and
727 washed in water. For antigen retrieval, slides were placed in staining jar containing 1X Citrate
728 Buffer (pH 6) for 15 minutes using a preheated pressure cooker (high pressure and high temp).
729 The tissue slides were washed with 1X TBS-T and blocked tissue sections with Buffer W for 1
730 hour at room temperature in a closed humidity chamber. Tissue slides were stained with a cocktail
731 of fluorescent morphological markers SYTO13 (nuclear stain; AF532), CD20 (Clone: L26; AF488),
732 CD3 (Clone: CD3-12; AF594), and Ki-67 (Clone: B56; AF647) at 1:10000, 1:250, 1:100, and

733 1:1000 dilutions, respectively. For protein detection, a multiplex cocktail of primary antibodies was
734 used from core panels; GeoMx immune cell profiling panel, GeoMx IO drug target module, and
735 GeoMx immune activation status module (S*ee supplementary Table2*). In total, 60 regions of
736 interest (ROIs) were selected within GCs based on co-localization of CD3 with CD20+ Ki-67+ GC
737 B cells. Indexing oligos were released from each ROI by exposure to UV light as described(Merritt,
738 Ong et al. 2020), and 10μl of liquid from above the ROI was collected by a microcapillary tip and
739 deposited in a 96-well plate.
740 Indexing oligos from each ROI were PCR amplified using GeoMx Seq Code primers. PCR
741 products were pooled and purified twice with AMPure XP beads (Beckman Coulter, Brea, CA).
742 Library concentration and purity were measured using a high-sensitivity DNA Bioanalyzer chip
743 (Agilent Technologies, Santa Clara, CA). Paired-end sequencing was performed on an Illumina
744 HiSeq 2000 instrument (Illumina, San Diego, CA). After sequencing, fastq files were run through
745 the GeoMx NGS Pipeline where reads were trimmed, merged, and aligned to a list of indexing
746 oligos to identify the source probe. Analysis of filtered normalized gene expression data was
747 performed in R with Bioconductor. We profiled 32 proteins along with core protein in GeoMx
748 Human Protein array. We first calculated the signal-to-noise ratio by dividing raw count values by
749 the geometric mean of the negative IgG probes. The data were normalized using three negative
750 control IgG probes with the GeomxTools package. Normalized expression values were used for
751 downstream analyses. Dimensionality reduction analysis was performed with principal
752 component analysis using the facomineR package(Lê, Josse et al. 2008). Differential expression
753 analysis was conducted with the mixedModelDE function from the GeomxTools package. We
754 tested for differences between time points and/or vaccine groups using linear mixed effect models
755 that incorporated animal ID as a random effect term to account for non-independence of the
756 multiple ROIs sampled per animal. Differential expression results were visualized in heatmap
757 plots generated using the ComplexHeatmap R package(Gu, Eils et al. 2016).
758

759 **Serum IgG ELISA**. Serum IgG titers against HIV-1 C.1086 Env gp140 were determined by ELISA
760 as described previously (Verma, Schmidt et al. 2019). In brief, 96-well microtiter plates with high
761 binding capacity (Thermo Fisher, USA) were coated overnight at 4°C with C.1086 Env gp140
762 protein from the NIH AIDS Reagent Program (ARP) diluted in coating buffer. Plates were washed
763 and blocked with nonfat dry milk in PBS for two hours at room temperature and washed five times
764 with 1X PBS-0.05% tween20 (PBST). Diluted standard and serum samples were added to plate
765 wells and incubated overnight at 4°C. Plates were washed, and HRP conjugated goat anti-
766 monkey IgG (Nordic MUbio, Netherlands) was added to plate wells and incubated at room
767 temperature for 1 hour. Plates were then washed and developed with the addition of TMB
768 substrate (Thermo Fisher, USA). Absorbance was recorded at 450 nm with a reference filter at
769 570 nm using a Spectramax 5 plate reader (Molecular Devices, USA). Baseline sera from each
770 animal served as negative control and optical density (OD) values 2-fold above baseline were
771 considered positive and extrapolated using in-plate standards to determine anti-Env antibody
772 concentrations.
773
774 **IgG subclass antibodies.** ELISA was used to measure concentrations of gp120-specific IgG1-4
775 antibodies. Ten rows of a 96-well Immulon 4 microtiter plate (VWR) were coated overnight at 4˚C
776 with 50ng C.1086 gp120Δ7 (HIV Reagent Program) per well in PBS, pH 7.2. To generate a
777 standard curve with a known amount of IgG1, IgG2, IgG3 or IgG4 antibody, 2 rows of the plate
778 were coated with 50ng per well recombinant CD40 (NHP Reagent Resource). The following day,
779 the plate was washed with PBST and blocked with PBST containing 0.1% BSA (ELISA buffer:
780 EB). Serum samples diluted in EB were then added to gp120 wells. Duplicate dilutions of anti-
781 CD40 rhesus IgG1, IgG2, IgG3 or IgG4 antibody (NHP Reagent Resource) were added to the
782 CD40 wells. Following overnight reaction at 4˚C, the plate was washed and treated for 1h at 37˚C
783 with 0.5μg/ml of the appropriate following biotinylated monoclonal antibody (all from NHP Reagent

784 Resource) diluted in EB: anti-rhesus IgG1 clone 7H11 (ena), anti-rhesus IgG2 clone 8D11 (dio),
785 anti-rhesus IgG3 clone 6F5 (tria) or anti-rhesus IgG4 clone 7A8 (tessera). Plates were washed,
786 treated with 1/4,000 neutralite avidin peroxidase (SouthernBiotech) for 30min at room
787 temperature, and developed with TMB substrate and H_2SO_4 stop solution. After recording
788 absorbance at 450nm, a standard curve constructed from the anti-CD40 IgG subclass antibody
789 was used to interpolate the concentration of anti-gp120 IgG of the same subclass in samples
790
791 **ADP assay.** Serum antibodies were evaluated for ability to enhance phagocytosis of gp120
792 expressing fluorescent beads by THP-1 monocytes as previously described (Verma 2020).
793 Briefly, 1µm avidin-coated fluorospheres (Invitrogen) were labeled with biotinylated anti-His tag
794 monoclonal antibody (ThermoScientific) and used to capture His-tagged clade C gp120 Du151
795 protein (Immune Technologies). The gp120-expressing beads were then incubated with
796 triplicate 5-fold dilutions of heat-inactivated serum samples in V-bottom plates for 1h at 37˚C.
797 THP-1 cells ($2x10^4$ per well) were then added and incubated at 37°C in 5% CO_2. After 5h, cells
798 were washed with $Ca^{+2/}Mg^{+2}$-free DPBS, then treated with 0.12% trypsin-EDTA for 5 min at
799 37°C. The cells were washed and resuspended in 1% paraformaldehyde. Fluorescence was
800 measured using a FACSCanto (BD Biosciences) and FlowJo 9 software. Phagocytosis was
801 quantified by multiplying the percentage of fluorescent cells by their median fluorescence
802 intensity. A phagocytic score was then calculated by dividing the phagocytosis measured in
803 each test sample by the phagocytosis observed for pooled preimmune serum at the same
804 dilution.
805
806 **Neutralization assay.** Serum neutralizing activity was quantified using a previously described
807 pseudovirus infectivity assay where TZM-bl cells were co-incubated with tier 1 clade C
808 pseudovirus MW965.26, tier 2 clade C virus Ce1086_B2, tier 2 clade C Ce1176_A3, or a control
809 MLV-pseudotyped virus (to measure non-HIV-specific activity). Neutralization titers were

810 measured in serum samples collected at week 0 and week 2 following the 2nd protein boost.
811 Samples neutralizing antibody activity against SIV pseudoviruses was measured relative to MLV
812 pseudovirus negative controls.
813
814 **Mucosal antibodies.** A custom binding antibody multiplex assay (BAMA) assay with C.1086
815 gp140 K160N-conjugated Bio-Rad Bio-plex Pro magnetic COOH beads was used to quantify Env-
816 specific IgG in rectal secretions and specific IgA in IgG-depleted sera and rectal secretions as
817 previously described (Verma, Schmidt et al. 2019). Briefly, 50µg gp140 was conjugated to 10 x
818 10^6 beads as described (Iyer, Gangadhara et al. 2015). The gp140-labeled beads (3500 per well)
819 were shaken overnight at 1100 rpm and 4˚C with 10-fold dilutions of serum or secretion and
820 standard [Verma 2020]. Beads were then washed with PBST and reacted for 30min at room
821 temperature with biotinylated goat anti-human IgG (Southern Biotech) or goat whole IgG
822 containing anti-monkey IgA (Novus) followed by phycoerythrin-labeled neutralite avidin (Southern
823 Biotech). Fluorescence was measured with a Bio-Rad Bioplex 200. Antibody concentrations were
824 determined using standard curves prepared with Bioplex Manager software (Bio-Rad).
825 Concentrations of gp120-specific IgG in secretions were divided by the concentration of total IgG
826 or IgA measured in the sample by ELISA to obtain the specific activity (ng of gp140-specific IgG
827 or IgA antibody per µg of total IgG or IgA, respectively).
828
829 **Statistical analysis.** Statistical analysis was performed using Prism v.9.5.1 (Graph Pad).
830 Gaussian distribution was not assumed, thus comparisons across time, between groups, and
831 correlations were analyzed using non-parametric tests. For within group comparisons, Wilcoxon
832 matched pairs signed rank test was used. For between group comparisons, Mann-Whitney rank
833 comparisons were used. Correlation coefficients were computed using Spearman correlation. P
834 values < 0.05 were considered significant.
835

REFERENCES

(2012). "clusterProfiler: an R Package for Comparing Biological Themes Among Gene Clusters." OMICS: A Journal of Integrative Biology **16**(5): 284-287.

Alving, C. R., K. K. Peachman, M. Rao and S. G. Reed (2012). "Adjuvants for human vaccines." Curr Opin Immunol **24**(3): 310-315.

Barbet, G., L. E. Sander, M. Geswell, I. Leonardi, A. Cerutti, I. Iliev and J. M. Blander (2018). "Sensing Microbial Viability through Bacterial RNA Augments T Follicular Helper Cell and Antibody Responses." Immunity **48**(3): 584-598 e585.

Carpenter, M. C. and M. E. Ackerman (2020). "Recent insights into Fc-mediated effector responses to HIV-1." Curr Opin HIV AIDS **15**(5): 282-289.

Christensen, D., L. Bollehuus Hansen, R. Leboux, W. Jiskoot, J. P. Christensen, P. Andersen and J. Dietrich (2019). "A Liposome-Based Adjuvant Containing Two Delivery Systems with the Ability to Induce Mucosal Immunoglobulin A Following a Parenteral Immunization." ACS Nano **13**(2): 1116-1126.

Cohen, K. W., Y. Tian, C. Thayer, A. Seese, R. Amezquita, M. J. McElrath, S. C. De Rosa and R. Gottardo (2022). "Th2-Biased Transcriptional Profile Predicts HIV Envelope-Specific Polyfunctional CD4(+) T Cells That Correlated with Reduced Risk of Infection in RV144 Trial." J Immunol **209**(3): 526-534.

Crotty, S. (2014). "T follicular helper cell differentiation, function, and roles in disease." Immunity **41**(4): 529-542.

Davidsen, J., I. Rosenkrands, D. Christensen, A. Vangala, D. Kirby, Y. Perrie, E. M. Agger and P. Andersen (2005). "Characterization of cationic liposomes based on dimethyldioctadecylammonium and synthetic cord factor from M. tuberculosis (trehalose 6,6'-dibehenate)-a novel adjuvant inducing both strong CMI and antibody responses." Biochim Biophys Acta **1718**(1-2): 22-31.

Dobin, A., C. A. Davis, F. Schlesinger, J. Drenkow, C. Zaleski, S. Jha, P. Batut, M. Chaisson and T. R. Gingeras (2013). "STAR: ultrafast universal RNA-seq aligner." Bioinformatics **29**(1): 15-21.

Eisinger, R. W. and A. S. Fauci (2018). "Ending the HIV/AIDS Pandemic(1)." Emerg Infect Dis **24**(3): 413-416.

Fabregat, A., K. Sidiropoulos, G. Viteri, O. Forner, P. Marin-Garcia, V. Arnau, P. D'Eustachio, L. Stein and H. Hermjakob (2017). "Reactome pathway analysis: a high-performance in-memory approach." BMC Bioinformatics **18**(1): 142.

Fauci, A. S. (2017). "An HIV Vaccine Is Essential for Ending the HIV/AIDS Pandemic." JAMA **318**(16): 1535-1536.

Felber, B. K., Z. Lu, X. Hu, A. Valentin, M. Rosati, C. A. L. Remmel, J. A. Weiner, M. C. Carpenter, K. Faircloth, S. Stanfield-Oakley, W. B. Williams, X. Shen, G. D. Tomaras, C. C. LaBranche, D. Montefiori, H. V. Trinh, M. Rao, M. S. Alam, N. A. Vandergrift, K. O. Saunders, Y. Wang, W. Rountree, J. Das, G. Alter, S. G. Reed, P. P. Aye, F. Schiro, B. Pahar, J. P. Dufour, R. S. Veazey, P. A. Marx, D. J. Venzon, G. M. Shaw, G. Ferrari, M. E. Ackerman, B. F. Haynes and G. N. Pavlakis (2020). "Co-immunization of DNA and Protein in the Same Anatomical Sites Induces Superior Protective Immune Responses against SHIV Challenge." Cell Rep **31**(6): 107624.

Fischinger, S., C. M. Boudreau, A. L. Butler, H. Streeck and G. Alter (2019). "Sex differences in vaccine-induced humoral immunity." Semin Immunopathol **41**(2): 239-249.

Gao, X., K. Luo, D. Wang, Y. Wei, Y. Yao, J. Deng, Y. Yang, Q. Zeng, X. Dong, L. Xiong, D. Gong, L. Lin, K. Pohl, S. Liu, Y. Liu, L. Liu, T. H. O. Nguyen, L. F. Allen, K. Kedzierska, Y. Jin, M. R. Du, W. Chen, L. Lu, N. Shen, Z. Liu, I. A. Cockburn, W. Luo and D. Yu (2023). "T follicular helper 17 (Tfh17) cells are superior for immunological memory maintenance." Elife **12**.

886 Gu, Z., R. Eils and M. Schlesner (2016). "Complex heatmaps reveal patterns and correlations in
887 multidimensional genomic data." Bioinformatics **32**(18): 2847-2849.
888 Hayashi, N., T. Yoshimoto, K. Izuhara, K. Matsui, T. Tanaka and K. Nakanishi (2007). "T helper
889 1 cells stimulated with ovalbumin and IL-18 induce airway hyperresponsiveness and lung
890 fibrosis by IFN-gamma and IL-13 production." Proc Natl Acad Sci U S A **104**(37): 14765-14770.
891 Henriksen-Lacey, M., D. Christensen, V. W. Bramwell, T. Lindenstrom, E. M. Agger, P.
892 Andersen and Y. Perrie (2011). "Comparison of the depot effect and immunogenicity of
893 liposomes based on dimethyldioctadecylammonium (DDA), 3beta-[N-(N',N'-
894 Dimethylaminoethane)carbomyl] cholesterol (DC-Chol), and 1,2-Dioleoyl-3-trimethylammonium
895 propane (DOTAP): prolonged liposome retention mediates stronger Th1 responses." Mol Pharm
896 **8**(1): 153-161.
897 Hill, D. L., W. Pierson, D. J. Bolland, C. Mkindi, E. J. Carr, J. Wang, S. Houard, S. W. Wingett,
898 R. Audran, E. F. Wallin, S. A. Jongo, K. Kamaka, M. Zand, F. Spertini, C. Daubenberger, A. E.
899 Corcoran and M. A. Linterman (2019). "The adjuvant GLA-SE promotes human Tfh cell
900 expansion and emergence of public TCRbeta clonotypes." J Exp Med.
901 Hirota, K., J. E. Turner, M. Villa, J. H. Duarte, J. Demengeot, O. M. Steinmetz and B. Stockinger
902 (2013). "Plasticity of Th17 cells in Peyer's patches is responsible for the induction of T cell-
903 dependent IgA responses." Nat Immunol **14**(4): 372-379.
904 Iyer, S. S., S. Gangadhara, B. Victor, R. Gomez, R. Basu, J. J. Hong, C. Labranche, D. C.
905 Montefiori, F. Villinger, B. Moss and R. R. Amara (2015). "Codelivery of Envelope Protein in
906 Alum with MVA Vaccine Induces CXCR3-Biased CXCR5+ and CXCR5- CD4 T Cell Responses
907 in Rhesus Macaques." J Immunol **195**(3): 994-1005.
908 Kumar, P., K. Chen and J. K. Kolls (2013). "Th17 cell based vaccines in mucosal immunity."
909 Curr Opin Immunol **25**(3): 373-380.
910 Lê, S., J. Josse and F. Husson (2008). "FactoMineR: An R Package for Multivariate Analysis."
911 Journal of Statistical Software **25**(1): 1 - 18.
912 Liao, Y., G. K. Smyth and W. Shi (2013). "featureCounts: an efficient general purpose program
913 for assigning sequence reads to genomic features." Bioinformatics **30**(7): 923-930.
914 Lin, L., G. Finak, K. Ushey, C. Seshadri, T. R. Hawn, N. Frahm, T. J. Scriba, H. Mahomed, W.
915 Hanekom, P.-A. Bart, G. Pantaleo, G. D. Tomaras, S. Rerks-Ngarm, J. Kaewkungwal, S.
916 Nitayaphan, P. Pitisuttithum, N. L. Michael, J. H. Kim, M. L. Robb, R. J. O'Connell, N.
917 Karasavvas, P. Gilbert, S. C De Rosa, M. J. McElrath and R. Gottardo (2015). "COMPASS
918 identifies T-cell subsets correlated with clinical outcomes." Nature Biotechnology **33**(6): 610-
919 616.
920 Love, M. I., W. Huber and S. Anders (2014). "Moderated estimation of fold change and
921 dispersion for RNA-seq data with DESeq2." Genome Biology **15**(12): 550.
922 Martinez-Lopez, M., S. Iborra, R. Conde-Garrosa, A. Mastrangelo, C. Danne, E. R. Mann, D. M.
923 Reid, V. Gaboriau-Routhiau, M. Chaparro, M. P. Lorenzo, L. Minnerup, P. Saz-Leal, E. Slack, B.
924 Kemp, J. P. Gisbert, A. Dzionek, M. J. Robinson, F. J. Ruperez, N. Cerf-Bensussan, G. D.
925 Brown, D. Bernardo, S. LeibundGut-Landmann and D. Sancho (2019). "Microbiota Sensing by
926 Mincle-Syk Axis in Dendritic Cells Regulates Interleukin-17 and -22 Production and Promotes
927 Intestinal Barrier Integrity." Immunity **50**(2): 446-461 e449.
928 McCausland, M. M., I. Yusuf, H. Tran, N. Ono, Y. Yanagi and S. Crotty (2007). "SAP regulation
929 of follicular helper CD4 T cell development and humoral immunity is independent of SLAM and
930 Fyn kinase." J Immunol **178**(2): 817-828.
931 Merritt, C. R., G. T. Ong, S. E. Church, K. Barker, P. Danaher, G. Geiss, M. Hoang, J. Jung, Y.
932 Liang, J. McKay-Fleisch, K. Nguyen, Z. Norgaard, K. Sorg, I. Sprague, C. Warren, S. Warren, P.
933 J. Webster, Z. Zhou, D. R. Zollinger, D. L. Dunaway, G. B. Mills and J. M. Beechem (2020).
934 "Multiplex digital spatial profiling of proteins and RNA in fixed tissue." Nature Biotechnology
935 **38**(5): 586-599.

936 Mitsdoerffer, M., Y. Lee, A. Jager, H. J. Kim, T. Korn, J. K. Kolls, H. Cantor, E. Bettelli and V. K.
937 Kuchroo (2010). "Proinflammatory T helper type 17 cells are effective B-cell helpers." Proc Natl
938 Acad Sci U S A **107**(32): 14292-14297.
939 Morita, R., N. Schmitt, S. E. Bentebibel, R. Ranganathan, L. Bourdery, G. Zurawski, E. Foucat,
940 M. Dullaers, S. Oh, N. Sabzghabaei, E. M. Lavecchio, M. Punaro, V. Pascual, J. Banchereau
941 and H. Ueno (2011). "Human blood CXCR5(+)CD4(+) T cells are counterparts of T follicular
942 cells and contain specific subsets that differentially support antibody secretion." Immunity **34**(1):
943 108-121.
944 Moyron-Quiroz, J. E., J. Rangel-Moreno, K. Kusser, L. Hartson, F. Sprague, S. Goodrich, D. L.
945 Woodland, F. E. Lund and T. D. Randall (2004). "Role of inducible bronchus associated
946 lymphoid tissue (iBALT) in respiratory immunity." Nat Med **10**(9): 927-934.
947 Olatunde, A. C., J. S. Hale and T. J. Lamb (2021). "Cytokine-skewed Tfh cells: functional
948 consequences for B cell help." Trends Immunol **42**(6): 536-550.
949 Ovsyannikova, I. G., N. Dhiman, R. M. Jacobson, R. A. Vierkant and G. A. Poland (2003).
950 "Frequency of measles virus-specific CD4+ and CD8+ T cells in subjects seronegative or highly
951 seropositive for measles vaccine." Clin Diagn Lab Immunol **10**(3): 411-416.
952 Ovsyannikova, I. G., K. C. Reid, R. M. Jacobson, A. L. Oberg, G. G. Klee and G. A. Poland
953 (2003). "Cytokine production patterns and antibody response to measles vaccine." Vaccine
954 **21**(25-26): 3946-3953.
955 Pedersen, G. K., P. Andersen and D. Christensen (2018). "Immunocorrelates of CAF family
956 adjuvants." Semin Immunol **39**: 4-13.
957 Pedersen, G. K., K. Wørzner, P. Andersen and D. Christensen (2020). "Vaccine Adjuvants
958 Differentially Affect Kinetics of Antibody and Germinal Center Responses." Frontiers in
959 Immunology **11**.
960 Rao, M., S. Onkar, K. K. Peachman, Y. White, H. V. Trinh, O. Jobe, Y. Zhou, P. Dawson, M. A.
961 Eller, G. R. Matyas and C. R. Alving (2018). "Liposome-Encapsulated Human Immunodeficiency
962 Virus-1 gp120 Induces Potent V1V2-Specific Antibodies in Humans." J Infect Dis **218**(10): 1541-
963 1550.
964 Slifka, M. K., R. Antia, J. K. Whitmire and R. Ahmed (1998). "Humoral immunity due to long-
965 lived plasma cells." Immunity **8**(3): 363-372.
966 Subramanian, A., P. Tamayo, V. K. Mootha, S. Mukherjee, B. L. Ebert, M. A. Gillette, A.
967 Paulovich, S. L. Pomeroy, T. R. Golub, E. S. Lander and J. P. Mesirov (2005). "Gene set
968 enrichment analysis: a knowledge-based approach for interpreting genome-wide expression
969 profiles." Proc Natl Acad Sci U S A **102**(43): 15545-15550.
970 Verma, A., B. A. Schmidt, S. R. Elizaldi, N. K. Nguyen, K. A. Walter, Z. Beck, H. V. Trinh, A. R.
971 Dinsarapu, Y. S. Lakshmanappa, N. N. Rane, G. R. Matyas, M. Rao, X. Shen, G. D. Tomaras,
972 C. C. LaBranche, K. A. Reimann, D. H. Foehl, J. S. Gach, D. N. Forthal, P. A. Kozlowski, R. R.
973 Amara and S. S. Iyer (2019). "Impact of Th1 CD4 TFH skewing on Antibody Responses to an
974 HIV-1 Vaccine in Rhesus Macaques." J Virol.
975 Ward, B. J. and D. E. Griffin (1993). "Changes in cytokine production after measles virus
976 vaccination: predominant production of IL-4 suggests induction of a Th2 response." Clin
977 Immunol Immunopathol **67**(2): 171-177.
978 Werninghaus, K., A. Babiak, O. Gross, C. Holscher, H. Dietrich, E. M. Agger, J. Mages, A.
979 Mocsai, H. Schoenen, K. Finger, F. Nimmerjahn, G. D. Brown, C. Kirschning, A. Heit, P.
980 Andersen, H. Wagner, J. Ruland and R. Lang (2009). "Adjuvanticity of a synthetic cord factor
981 analogue for subunit Mycobacterium tuberculosis vaccination requires FcRgamma-Syk-Card9-
982 dependent innate immune activation." J Exp Med **206**(1): 89-97.
983 Wørzner, K., J. Hvannastein, S. T. Schmidt, C. Foged, I. Rosenkrands, G. K. Pedersen and D.
984 Christensen (2021). "Adsorption of protein antigen to the cationic liposome adjuvant CAF®01 is
985 required for induction of Th1 and Th17 responses but not for antibody induction." Eur J Pharm
986 Biopharm **165**: 293-305.

Acknowledgements

The authors are grateful to Dennis Christensen, previously at the SSI, for provision of CAF01 adjuvant for the studies. The authors are grateful to Brian Schmidt for technical assistance with the LAMV study; Wilhelm Von Morgenland and Miles Christensen and the CNPRC SAIDS team for coordination of macaque studies; Stephenie Liu at the UC Davis Genomics Resource for optimization of morphological markers for spatial profiling, and Daniel Newhouse at the Spatial Data Analysis Service (sDAS) for analysis of spatial proteomics data. We thank Robert L. Wilson for excellent technical assistance in processing secretions and measuring mucosal antibodies. The authors acknowledge funding support from NIAID, NIH R56AI150409 (SSI) ; Duke CFAR Grant P30 AI064518 (GDT). Reagents for measurement of rhesus IgG subclasses were obtained from the NIH Nonhuman Primate Reagent Resource supported by AI126683 and OD10976.

Data and materials availability

RNA-seq dataset is accessible at GSE234813 (submission in progress).

FIGURE LEGENDS

Figure 1. GC $T_{fh}1$ and GC $T_{fh}17$ cells recalled by measles booster. (**A**) Overview of study design; adult female rhesus macaques immunized with Live Attenuated Measles Virus vaccine (LAMV). **(B)** Serum MeV IgG kinetics measured by ELISA. **(C)** Avidity index (AI) of MeV IgG measured using chaotropic displacement ELISA with sodium thiocyanate at week 20 and week 0 in serum. **(D)** Representative flow cytometry plots showing $ICOS^+Ki\text{-}67^+$ pT_{fh} cells in blood at day 0 and day 7 post LAMV. Kinetics of $ICOS^+Ki\text{-}67^+$ pT_{fh} cells. **(E)** Correlation between ICOS+ Ki-67+pT_{fh} cells at day 7 and MeV IgG at week 20. **(F)** T_h profile of pT_{fh} cells shows induction of $CXCR3^+$ $pT_{fh}1$ at day 7. **(G)** Boolean analysis (n=16) shows $pT_{fh}1$ cells induced 1 week post LAMV. **(H)** Representative flow cytometry plots show $CXCR5^+$ $PD\text{-}1^{++}$ GC T_{fh} cells and histogram shows Bcl-6 expression on GC T_{fh} cells. T_h profile of GC T_{fh} cells shows expression of CXCR3 and CCR6. **(I)** Boolean analysis (n=14) shows proportion of T_h1, T_h17 and $T_h1/17$ GC T_{fh} subsets.

1013 **(J)** Bubble plots show genes for significantly enriched pathways related to T helper differentiation
1014 on sorted CXCR5+ PD-1+/++ cells. **(K)** Gene expression on sorted CXCR5+ PD-1+/++ cells.
1015 Statistical analysis was performed using two-tailed Wilcoxon matched-pairs signed rank test (in
1016 panels B-D, F) or spearman rank correlation test (E); * $p<0.05$, ** $p \leq 0.01$, *** $p \leq 0.001$, **** $p \leq$
1017 0.0001.
1018
1019 **Figure 2. Induction of Robust T Cell Activation in GCs with HIV-1 Env Formulated in CAF01**
1020 **and MPLA+QS-21 Adjuvants. (A)** Overview of experimental design for *in-situ* proteomics and
1021 transcriptional analysis. **(B)** Representative images of GC from FFPE sections of inguinal LN at
1022 baseline and week 2 post protein 1 immunization with HIV-Env gp140 | MPLA+QS-21; scale bar;
1023 top, 3mm, close up, 300 µm. LN sections were stained for CD20 (blue), CD3 (yellow), Ki-67
1024 (magenta), and DNA (gray) to identify GCs. Circular ROIs (100 µm in diameter, total 60) were
1025 selected based on co-localization of CD3 with CD20+ Ki-67+ GC B cells for proteomic profiling
1026 with a 32-plex antibody cocktail. Normalized protein expression (NPE) values were calculated
1027 using three negative control IgG probes. **(C)** NPE of key lineage markers across all ROIs at BL,
1028 P1w2, and P2w3. **(D-E)** Volcano plots show proteins induced post boost in each vaccine group.
1029 **(F)** Violin plots show common proteins induced post protein boost in MPLA and CAF01 groups.
1030 **(G)** Violin plots of proteins induced with CAF01 and MPLA. **(H)** Volcano plot (left) and Violin plots
1031 (right) of proteins significantly different across HIV-1 Env gp140 MPLA+QS-21 and CAF01
1032 regimens. Differential expression was modeled using a linear mixed-effect model to account for
1033 the sampling of multiple ROI/AOI segments per patient/tissue. Criterion of significance was
1034 nominal p value < 0.05, plots show False discovery rate (FDR).
1035
1036 **Figure 3. T_h1 molecular programs potentiated by HIV-1 Env/MPLA+QS-21. (A)** FACS
1037 purified CD95- (naive [N]) and CD95+ CD4 T cells, stimulated overnight with HIV-1 Env, were
1038 sequenced to assess transcriptional programs. (**B**) Principal component analysis (PCA) of all

1039 expressed genes shows distinct clustering of N and CD95+ cells. (**C**) Violin plots show transcripts
1040 per million values of differentially expressed transcription factors (p adj < 0.05) in CD95+ CD4 T
1041 cells relative to naive CD4 T cells post vaccination. (**D**) Bubble plots depict DEG at P1w2 versus
1042 BL in CD95+ CD4 T cells in CAF01 (top) and MPLA (bottom). Venn Diagram of DEG genes
1043 upregulated in CD95+ and naive subsets at P1w2 relative to BL shows 45 and 333 genes
1044 exclusively upregulated in CD95+ CD4 T cells with MPLA and CAF01, respectively. (**E**) Venn
1045 diagram of significantly downregulated genes. **(F)** PCA of all expressed genes shows distinct
1046 clustering across vaccine groups at P1w2. **(G**) Heat maps depict $\log_2$ gene expression (transcripts
1047 per million (TPM)) for highly DEG in CD95+ cells compared to naive cells at P1w2 in MPLA; heat
1048 map in inset depicts TPM of genes represented in Cytokine-cytokine receptor interaction
1049 pathways across vaccine regimens. (**H)** Chord plot shows GO Terms enriched with corresponding
1050 upregulated genes in CD95+ CD4 T cells at P1w2 with MPLA. **(I**) Heat maps depict $\log_2$ gene
1051 expression (TPM) for highly DEG in CD95+ cells compared to naive cells at P1w2 in CAF01; heat
1052 map in inset depicts TPM of genes represented in Cytokine-cytokine receptor interaction pathway
1053 across vaccine regimens.
1054
1055 **Figure 4. Phenotypically and functionally specialized GC $T_{fh}1$ / $T_{fh}17$ subsets elicited with**
1056 **HIV-1 Env Formulated in CAF01 and MPLA+QS-21 Adjuvants. (A)** Representative flow
1057 cytometry plot illustrates GC T_{fh} cells, GC T_{fh} frequencies (%CD95) (below) **(B)** flow cytometry plot
1058 shows identification of GC $T_{fh}1$, $T_{fh}17$, and $T_{fh}1/17$ cells with kinetics expressed as %CD95+ on
1059 the bottom. **(C)** Boolean analysis (n=6 each group) shows proportion of T_h1, T_h17 and $T_h1/17$ GC
1060 T_{fh} subsets. **(D-E)** Intracellular cytokine staining (ICS) analysis of T_h1, $T_{fh}17$, $T_{fh}1/17$ subsets at
1061 P1w2. **(F)** Gating strategy (left) and frequencies (right) of peripheral T_{fh} (pT_{fh}) and $pT_{fh}1$ cells in
1062 whole blood at P1w0 and P1w1. **(G)** Gating strategy (left) and frequencies (right) of activated
1063 ($CD40L^+OX40^+$) pT_{fh} ($CXCR5^+$) and non-pT_{fh} CD4 T cells (CXCR5-) cells in PBMCs at P1w1. **(H)**
1064 ICS of pT_{fh} and non-pT_{fh} CD4 T cells following Env stimulation at P1w1 and P2w1. Data points

1065 show individual animals. Statistical analysis was performed using two-tailed Wilcoxon matched-
1066 pairs signed rank test (in panels A-B, E) or Mann-Whitney U test (in panels C,D; F-G); * $p<0.05$,
1067 **$p \leq 0.01$.
1068
1069 **Figure 5. Induction of persistent anti-Env IgG antibodies with HIV-1 Env/MPLA+QS-21 (A)**
1070 Kinetics of HIV-1 Env IgG post protein boost (P1 and P2) across vaccine regimens measured by
1071 ELISA against C. 1086 gp140. **(B)** Serum gp140 IgG week 30 post P2w3. (**C**) GC $T_{fh}1$ cells
1072 correlate with gp140 IgG at week 30. **(D)** Env-specific (IFN-g^+IL-2^+) T_{fh} cells correlate with gp140
1073 IgG at week 30. **(E-I)** Area under the curve (AUC) values of IgG temporally shown by antigens,
1074 as indicated. (**J**) Temporal and (**K**) week 8 measures of gp140-specific IgG levels relative to total
1075 IgG in rectal secretions. Data points show individual animals. Statistical analysis was performed
1076 using Mann-Whitney U test (in panels A-B, E-K), or two-tailed Spearman rank correlation test (C-
1077 D); * $p<0.05$, **$p \leq 0.01$.
1078
1079 **Figure 6. Induction of IgG1 subclass antibodies with greater effector functions with HIV-1**
1080 **Env/MPLA+QS-21.** Serum C. 1086 gp120-specific (**A)** IgG1, **(B**) IgG2 **(C)** IgG4 antibodies at
1081 week 2 P2w3. **(D-E)** Antibody-dependent phagocytosis (ADP) score at 8 weeks post P2w3. **(F)**
1082 C. 1086 gp120-specific IgG1 correlates with ADP score. **(G)** Infectious dose 50% (ID50) titers to
1083 Tier 1A Clade C MW965.26 HIV-1 isolate. **(H-L)** Avidity index (with sodium citrate) across vaccine
1084 regimens against specific antigens. Data points show individual animals. Statistical analysis was
1085 performed using two-tailed Mann-Whitney U test (in panels A-E; G-L), or two-tailed Spearman
1086 rank correlation test (F); * $p<0.05$, **$p \leq 0.01$.
1087
1088 **Figure 7. Differentiation of GC T_{fh} Subsets initiated during the DNA Priming Phase. (A)**
1089 Experimental design of DNA immunization phase; FNA, lymph node fine needle aspirates.**(B)**
1090 Intracellular expression of Gag (2F12), surface expression of HIV-1 Env (PGT121) and IP10 and

1091 IL6 in supernatants of transfected 293T cells. **(C)** Flow cytometry plots show activated (PD-1$^+$Ki-
1092 67$^+$) pT_{fh} cells, frequencies post DNA3 (right top); frequencies of pT_{fh}1 cells (right bottom). **(D)** GC
1093 T_{fh} cells **(E)** Ki-67$^+$ PD1$^+$ cells of CXCR5+ in lymph node. **(F)** CXCR3+ subset of Ki-67$^+$ PD-1$^+$
1094 CXCR5$^+$ subset. (**G**) Ki-67+ PD-1+ T_{fh} in LN correlate with gp140 IgG at week 4 post DNA3 (**H**)
1095 Ki-67+ PD-1+ T_{fh}1 in LN correlate with gp140 IgG at week 4 post DNA **(I)** gp140 IgG at week 2
1096 post P1 correlates with gp140 IgG at week 4 post DNA3. Data points show individual animals.
1097 Statistical analysis was performed using one-tailed Wilcoxon matched-pairs signed rank test (in
1098 panels C-F), or Spearman rank correlation test (G-I); * $p<0.05$.
1099
1100 **S1, Supplement to Figure 1.**
1101 (**A**). Gating strategy to identify CXCR5$^+$ OX40$^+$ CD25$^+$ MeV-specific T_{fh} cells within PBMCs
1102 following stimulation with MeV antigen at Day 0 and Day 7 post LAMV. Right panel illustrates the
1103 MeV specific responses in CD4 T cells (%CD95) at weeks 0, 1, and 8 following immunization.
1104 (**B**). Flow plots illustrate gating strategy to identify pTfh cells. (**C**). Representative histograms show
1105 expression of TIGIT, CD200, CXCR3, CCR6, and CCR4 on GC Tfh cells in LN. (**D**). Sorting
1106 schematic to isolate CXCR5+ PD-1+/++ cells for RNA sequencing.
1107 **S2.** Experimental design of DNA-prime/Protein-boost Clade C HIV-1 immunization.
1108
1109 **S3, Supplement to Figure 2.** Sequencing QC histograms show (**A**) Signal-to-noise ratio
1110 computed by dividing raw count values by the geometric mean of the negative IgG probes. Quality
1111 control metrics- (**B**) deduplicated reads, (**C**) percent aligned reads, **(D)** sequencing saturation. (**E)**
1112 Bubble plot shows correlation of CD20 protein expression with CD4; bubble size corresponds to
1113 PD-1 expression, color intensity, Ki-67 expression; Spearman value, two-tailed p value of 60 pairs
1114 **(F)** Bubble plot shows correlation of CD4 protein expression with 4-1BB; bubble size corresponds
1115 to ICOS expression, color intensity, STING expression; Spearman value, two-tailed p value of 60

1116 pairs. **(G)** Heatmap plots show unsupervised hierarchical clustering of z-score values for each
1117 protein across time for each animal.
1118 **S4, Supplement to Figure 3. (A-B)** QC metrics **(C)** Bar graph shows DEG genes within CD4
1119 subsets post vaccination relative to baseline. (**D**) PCA plot of CD95+ CD4 T cell subsets at P2w3
1120 (**E**) Bubble plots show DEG enriched in CD95+ subsets at P1 in CAF01 and MPLA. GO-Terms of
1121 biological pathways differential induced in MPLA (**F**) and CAF01 (**G**) in CD95+ CD4 T cells at
1122 P1w2.
1123
1124 **S5, Supplement to Figure 4. (A)** Illustrates gating strategy to identify GC T_{fh} cells. **(B)**
1125 Frequencies of T_{fh} cells ($CD4^+CD95^+PD\text{-}1^+CXCR5^+$) (Top), $T_{fh}1$ cells ($CD4^+CD95^+PD\text{-}$
1126 $1^+CXCR5^+CXCR3^+$) (Middle), and $T_{fh}1/17$ cells ($CD4^+CD95^+PD\text{-}1^+CXCR5^+CXCR3^+CCR6^+$) in
1127 lymph nodes. **(C)** Intracellular cytokine staining (ICS) to identify Env-specific T_{fh} cells. (**D**). Co-
1128 expression of IL-2 and TNFa in IFNG+ versus IFNG- subsets producing IL-21. **(E)** Serum IL-21
1129 post P1 **(F)** Gating of AIM assay
1130
1131 **S6, Supplement to Figure 6.** Serum C. 1086 gp120-specific IgG1 (grey), IgG2 (pink), and IgG4
1132 (black) in animals (x-axis – animal IDs) P2w3
1133
1134 **S7, Supplement to Figure 7.** Frequencies of $OX40^+CD40L^+$ pT_{fh} cells stimulated ex vivo with
1135 Gag and Env.
1136
1137
1138
1139
1140
1141
1142
1143
1144
1145
1146

Figure 1

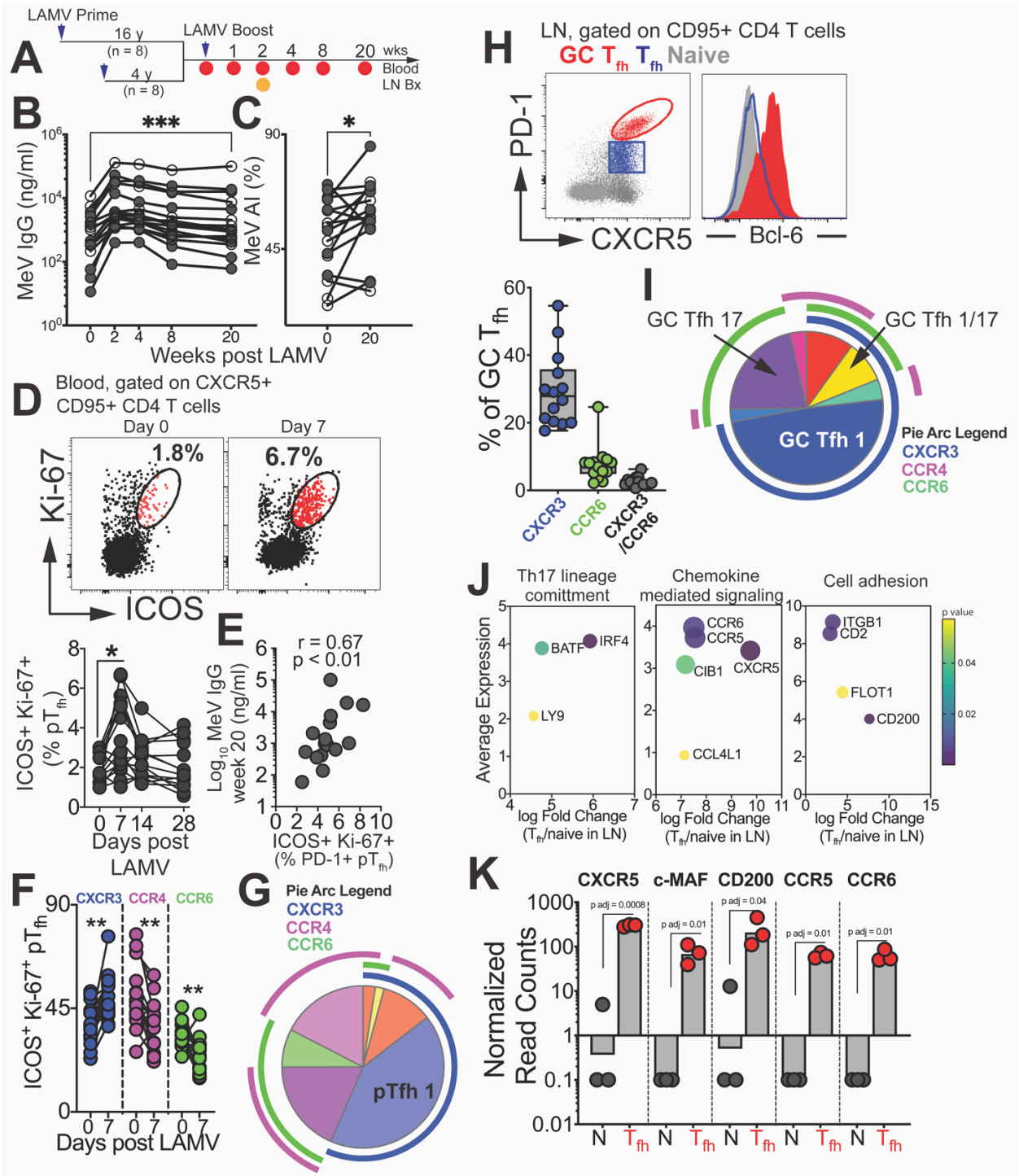
A
LAMV Prime
16 y
(n = 8)
4 y
(n = 8)
LAMV Boost
1 2 4 8 20 wks
Blood
LN Bx
B
MeV IgG (ng/ml)
Weeks post LAMV
C
MeV AI (%)
D
Blood, gated on CXCR5+
CD95+ CD4 T cells
Day 0
Day 7
1.8%
6.7%
Ki-67
ICOS
ICOS+ Ki-67+
(% pTfh)
Days post
LAMV
E
r = 0.67
p < 0.01
Log10 MeV IgG
week 20 (ng/ml)
ICOS+ Ki-67+
(% PD-1+ pTfh)
F
CXCR3 CCR4 CCR6
ICOS+ Ki-67+ pTfh
Days post LAMV
G
Pie Arc Legend
CXCR3
CCR4
CCR6
pTfh 1
H
LN, gated on CD95+ CD4 T cells
GC Tfh Tfh Naive
PD-1
CXCR5
Bcl-6
% of GC Tfh
CXCR3
CCR6
CXCR3
/CCR6
I
GC Tfh 17
GC Tfh 1/17
GC Tfh 1
Pie Arc Legend
CXCR3
CCR4
CCR6
J
Th17 lineage
comittment
Chemokine
mediated signaling
Cell adhesion
Average Expression
BATF
IRF4
LY9
CCR6
CCR5
CXCR5
CIB1
CCL4L1
ITGB1
CD2
FLOT1
CD200
p value
log Fold Change
(Tfh/naive in LN)
K
CXCR5 c-MAF CD200 CCR5 CCR6
Normalized
Read Counts
p adj = 0.0008
p adj = 0.01
p adj = 0.04
p adj = 0.01
p adj = 0.01
N Tfh N Tfh N Tfh N Tfh N Tfh

Figure 2

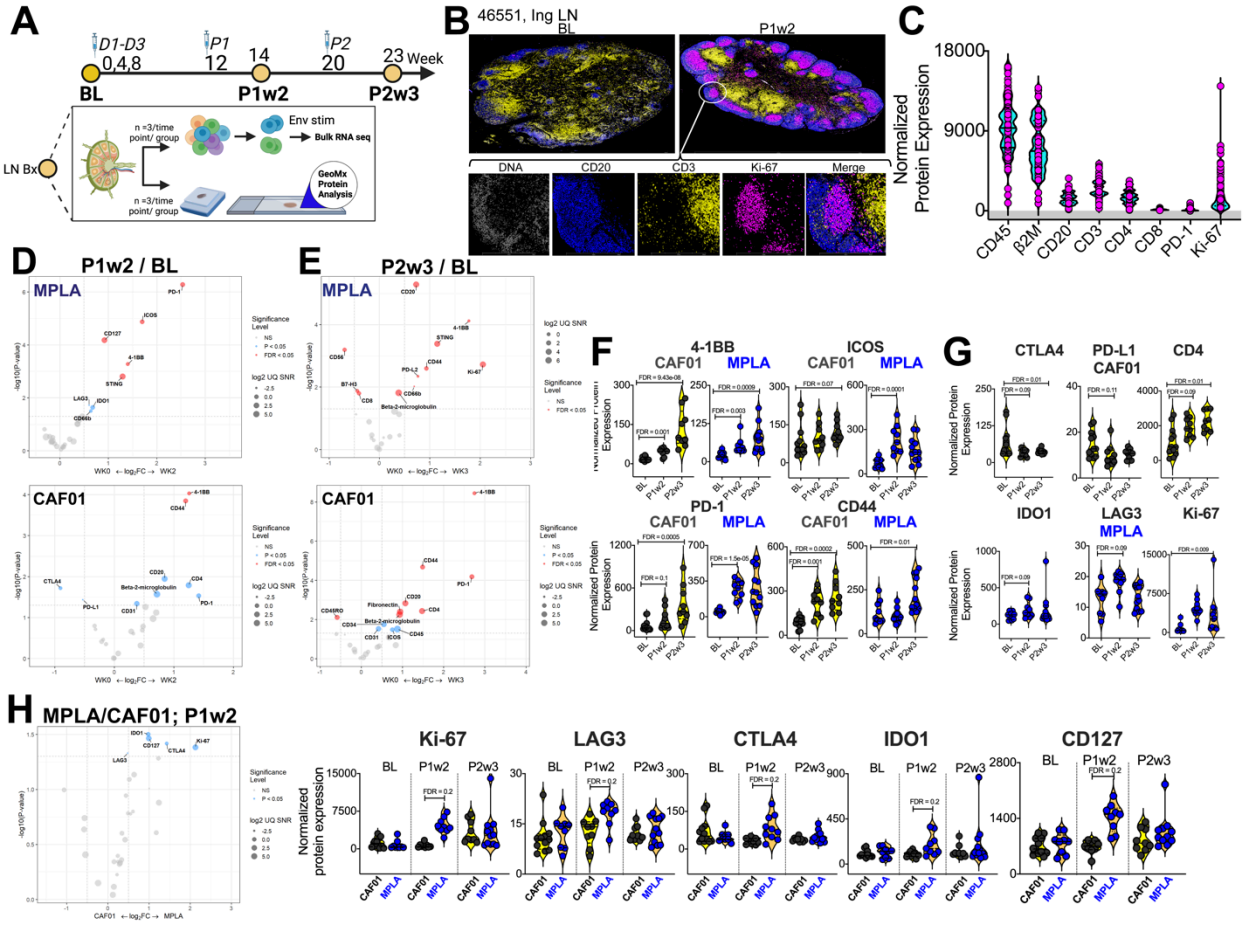
A
D1-D3
0,4,8
P1
12
14
P2
20
23 Week
BL
P1w2
P2w3
LN Bx
n =3/time point/ group
Env stim
Bulk RNA seq
GeoMx Protein Analysis
B
46551, Ing LN
BL
P1w2
DNA
CD20
CD3
Ki-67
Merge
C
Normalized Protein Expression
18000
9000
0
CD45
β2M
CD20
CD3
CD4
CD8
PD-1
Ki-67
D
P1w2 / BL
MPLA
CAF01
E
P2w3 / BL
MPLA
CAF01
F
4-1BB
ICOS
PD-1
CD44
CAF01
MPLA
Normalized Protein Expression
G
CTLA4
PD-L1
CD4
IDO1
LAG3
Ki-67
H
MPLA/CAF01; P1w2
Ki-67
LAG3
CTLA4
IDO1
CD127
BL
P1w2
P2w3
Normalized protein expression

Figure 3

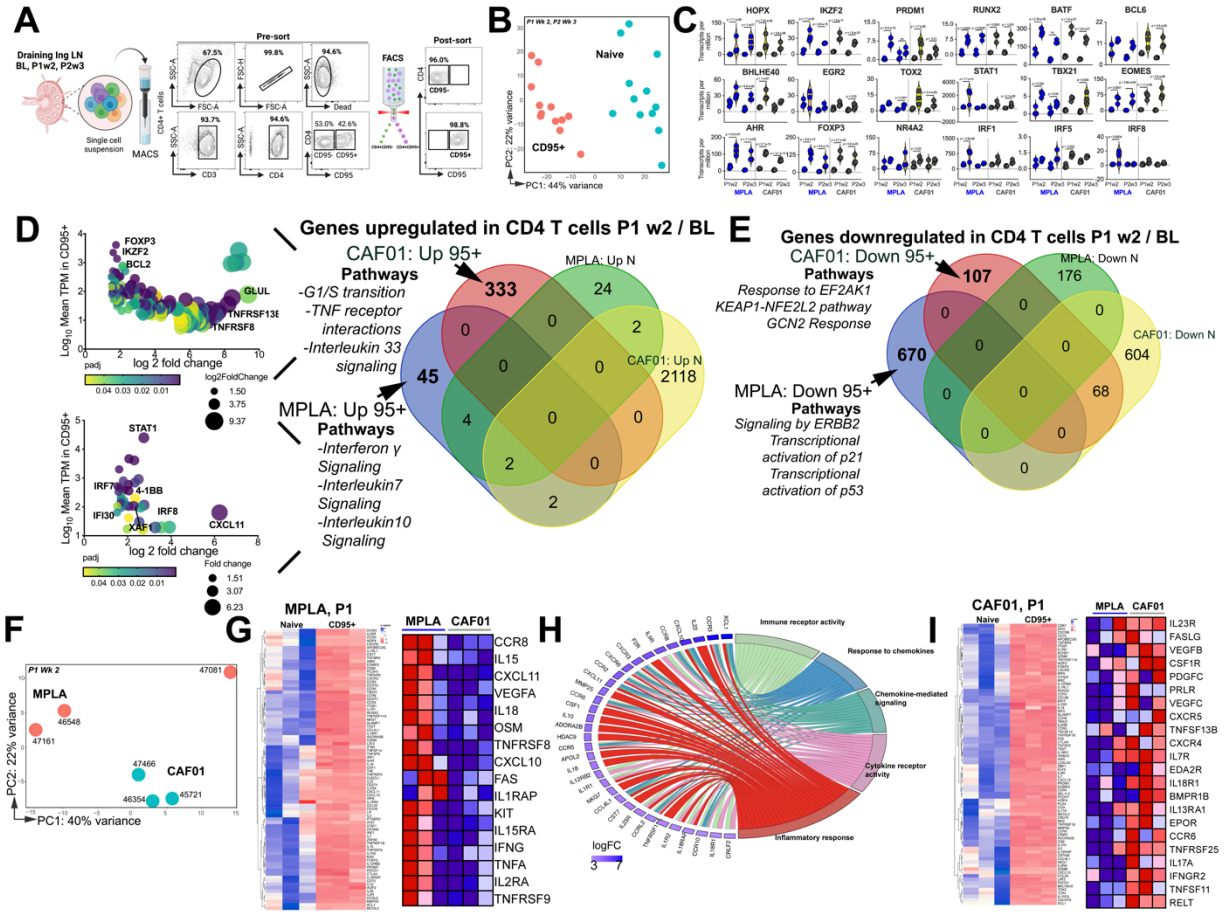
A
Draining Ing LN BL, P1w2, P2w3
Single cell suspension
MACS
CD4+ T cells
Pre-sort
Post-sort
FACS
B
P1 Wk 2, P2 Wk 3
Naive
CD95+
PC2: 22% variance
PC1: 44% variance
C
HOPX
IKZF2
PRDM1
RUNX2
BATF
BCL6
BHLHE40
EGR2
TOX2
STAT1
TBX21
EOMES
AHR
FOXP3
NR4A2
IRF1
IRF5
IRF8
MPLA
CAF01
D
Genes upregulated in CD4 T cells P1 w2 / BL
CAF01: Up 95+
Pathways
-G1/S transition
-TNF receptor interactions
-Interleukin 33 signaling
MPLA: Up 95+
Pathways
-Interferon γ Signaling
-Interleukin7 Signaling
-Interleukin10 Signaling
MPLA: Up N
CAF01: Up N
333
24
45
2118
E
Genes downregulated in CD4 T cells P1 w2 / BL
CAF01: Down 95+
Pathways
Response to EF2AK1 KEAP1-NFE2L2 pathway
GCN2 Response
MPLA: Down 95+
Pathways
Signaling by ERBB2
Transcriptional activation of p21
Transcriptional activation of p53
MPLA: Down N
CAF01: Down N
107
176
670
604
68
F
P1 Wk 2
MPLA
CAF01
PC2: 22% variance
PC1: 40% variance
G
MPLA, P1
Naive
CD95+
MPLA
CAF01
CCR8
IL15
CXCL11
VEGFA
IL18
OSM
TNFRSF8
CXCL10
FAS
IL1RAP
KIT
IL15RA
IFNG
TNFA
IL2RA
TNFRSF9
H
Immune receptor activity
Response to chemokines
Chemokine-mediated signaling
Cytokine receptor activity
Inflammatory response
logFC
I
CAF01, P1
Naive
CD95+
MPLA
CAF01
IL23R
FASLG
VEGFB
CSF1R
PDGFC
PRLR
VEGFC
CXCR5
TNFSF13B
CXCR4
IL7R
EDA2R
IL18R1
BMPR1B
IL13RA1
EPOR
CCR6
TNFRSF25
IL17A
IFNGR2
TNFSF11
RELT

Figure 4

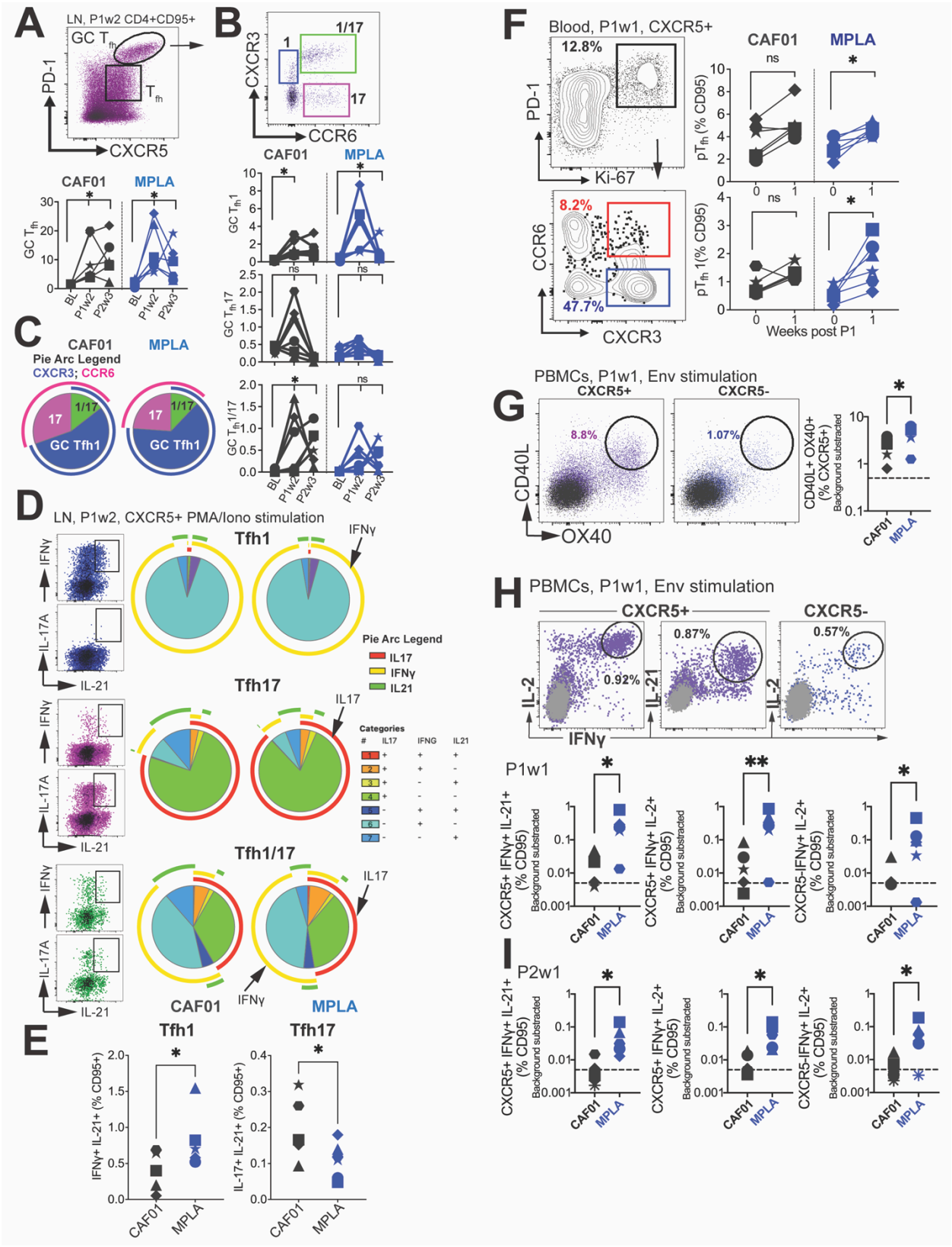
A
LN, P1w2 CD4+CD95+
GC Tfh
Tfh
PD-1
CXCR5
B
CXCR3
CCR6
1
1/17
17
CAF01
MPLA
GC Tfh
GC Tfh1
GC Tfh17
GC Tfh1/17
BL
P1w2
P2w3
ns
C
CAF01
MPLA
Pie Arc Legend
CXCR3; CCR6
17
1/17
GC Tfh1
D
LN, P1w2, CXCR5+ PMA/Iono stimulation
IFNγ
IL-17A
IL-21
Tfh1
Tfh17
Tfh1/17
Pie Arc Legend
IL17
IFNγ
IL21
Categories
E
Tfh1
Tfh17
IFNγ+ IL-21+ (% CD95+)
IL-17+ IL-21+ (% CD95+)
F
Blood, P1w1, CXCR5+
12.8%
PD-1
Ki-67
8.2%
47.7%
CCR6
CXCR3
pTfh (% CD95)
pTfh 1(% CD95)
Weeks post P1
G
PBMCs, P1w1, Env stimulation
CXCR5+
CXCR5-
8.8%
1.07%
CD40L
OX40
CD40L+ OX40+ (% CXCR5+)
Background substracted
H
PBMCs, P1w1, Env stimulation
CXCR5+
CXCR5-
0.87%
0.57%
0.92%
IL-2
IL-21
IFNγ
P1w1
CXCR5+ IFNγ+ IL-21+ (% CD95)
CXCR5+ IFNγ+ IL-2+ (% CD95)
CXCR5-IFNγ+ IL-2+ (% CD95)
I
P2w1

Figure 5

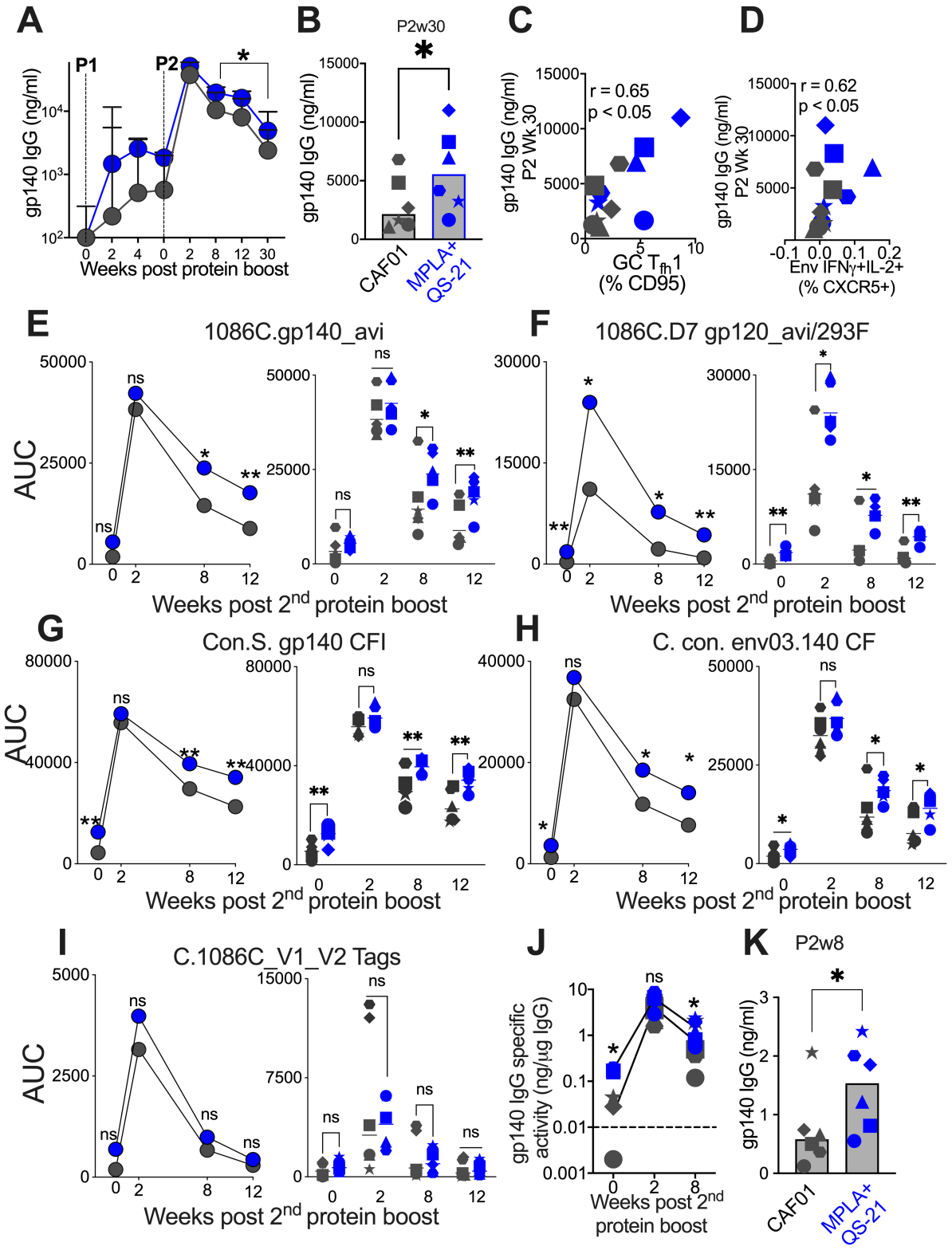
A
P1
P2
gp140 IgG (ng/ml)
Weeks post protein boost
B
P2w30
gp140 IgG (ng/ml)
CAF01
MPLA+ QS-21
C
r = 0.65
p < 0.05
gp140 IgG (ng/ml) P2 Wk 30
GC Tfh1 (% CD95)
D
r = 0.62
p < 0.05
gp140 IgG (ng/ml) P2 Wk 30
Env IFNγ+IL-2+ (% CXCR5+)
E
1086C.gp140_avi
AUC
Weeks post 2nd protein boost
F
1086C.D7 gp120_avi/293F
Weeks post 2nd protein boost
G
Con.S. gp140 CFI
AUC
Weeks post 2nd protein boost
H
C. con. env03.140 CF
Weeks post 2nd protein boost
I
C.1086C_V1_V2 Tags
AUC
Weeks post 2nd protein boost
J
gp140 IgG specific activity (ng/μg IgG)
Weeks post 2nd protein boost
K
P2w8
gp140 IgG (ng/ml)
CAF01
MPLA+ QS-21

1211 Figure 6
1212

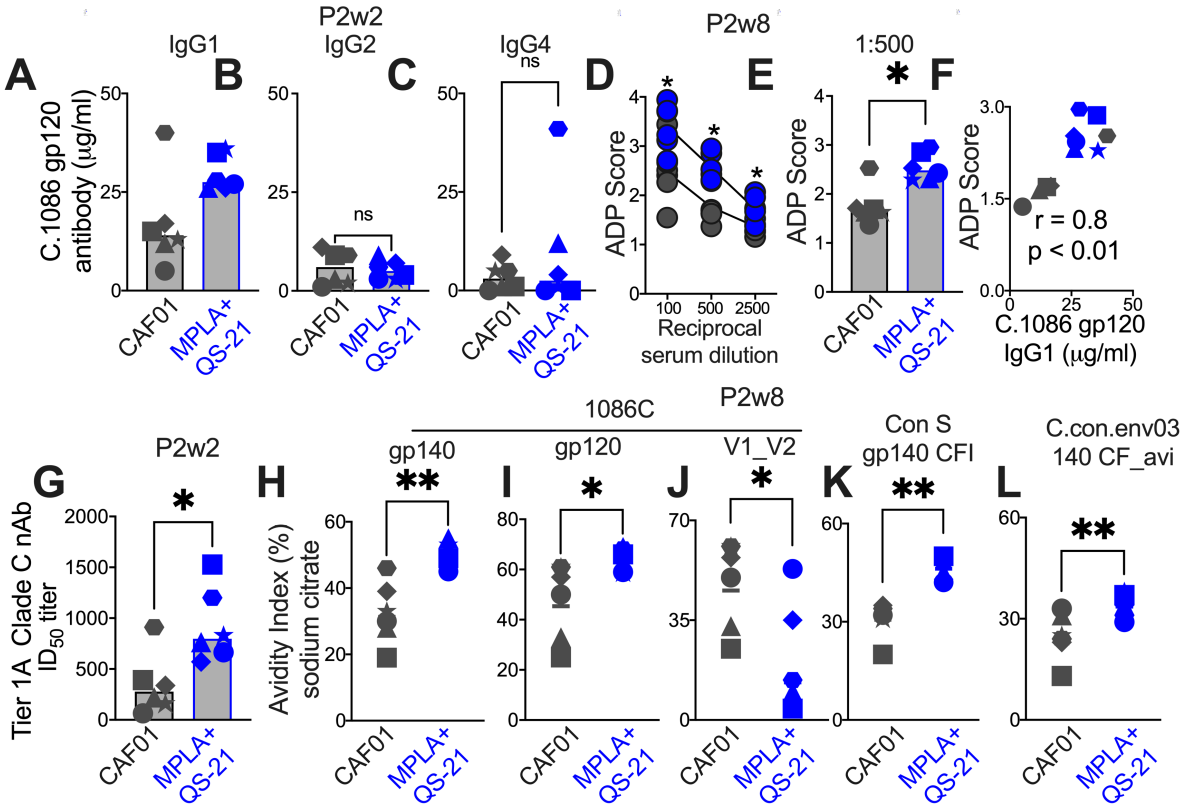

1213
1214
1215
1216
1217
1218
1219
1220
1221
1222
1223
1224
1225
1226
1227
1228
1229
1230
1231
1232
1233
1234
1235
1236
1237

Figure 7

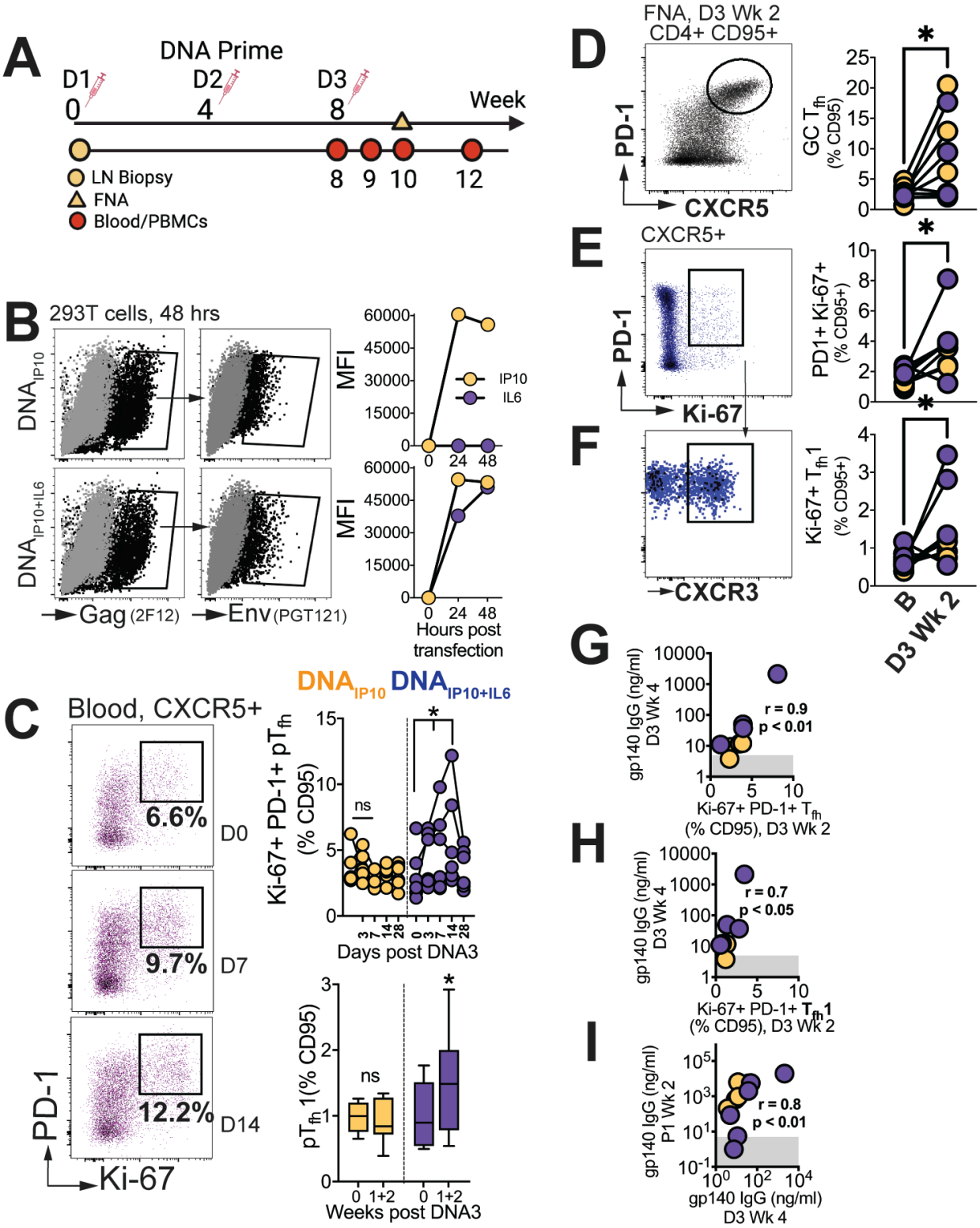
A
DNA Prime
D1
D2
D3
0
4
8
Week
LN Biopsy
FNA
Blood/PBMCs
8 9 10 12
B
293T cells, 48 hrs
DNA IP10
DNA IP10+IL6
Gag (2F12)
Env (PGT121)
MFI
IP10
IL6
Hours post transfection
C
Blood, CXCR5+
6.6%
D0
9.7%
D7
12.2%
D14
PD-1
Ki-67
DNA IP10
DNA IP10+IL6
Ki-67+ PD-1+ pTfh (% CD95)
ns
Days post DNA3
pTfh1(% CD95)
Weeks post DNA3
D
FNA, D3 Wk 2
CD4+ CD95+
PD-1
CXCR5
GC Tfh (% CD95)
E
CXCR5+
Ki-67
PD1+ Ki-67+ (% CD95+)
F
CXCR3
Ki-67+ Tfh1 (% CD95+)
B
D3 Wk 2
G
gp140 IgG (ng/ml) D3 Wk 4
r = 0.9
p < 0.01
Ki-67+ PD-1+ Tfh (% CD95), D3 Wk 2
H
r = 0.7
p < 0.05
Ki-67+ PD-1+ Tfh1 (% CD95), D3 Wk 2
I
gp140 IgG (ng/ml) P1 Wk 2
r = 0.8
p < 0.01
gp140 IgG (ng/ml) D3 Wk 4

S1, Supplement to Figure 1

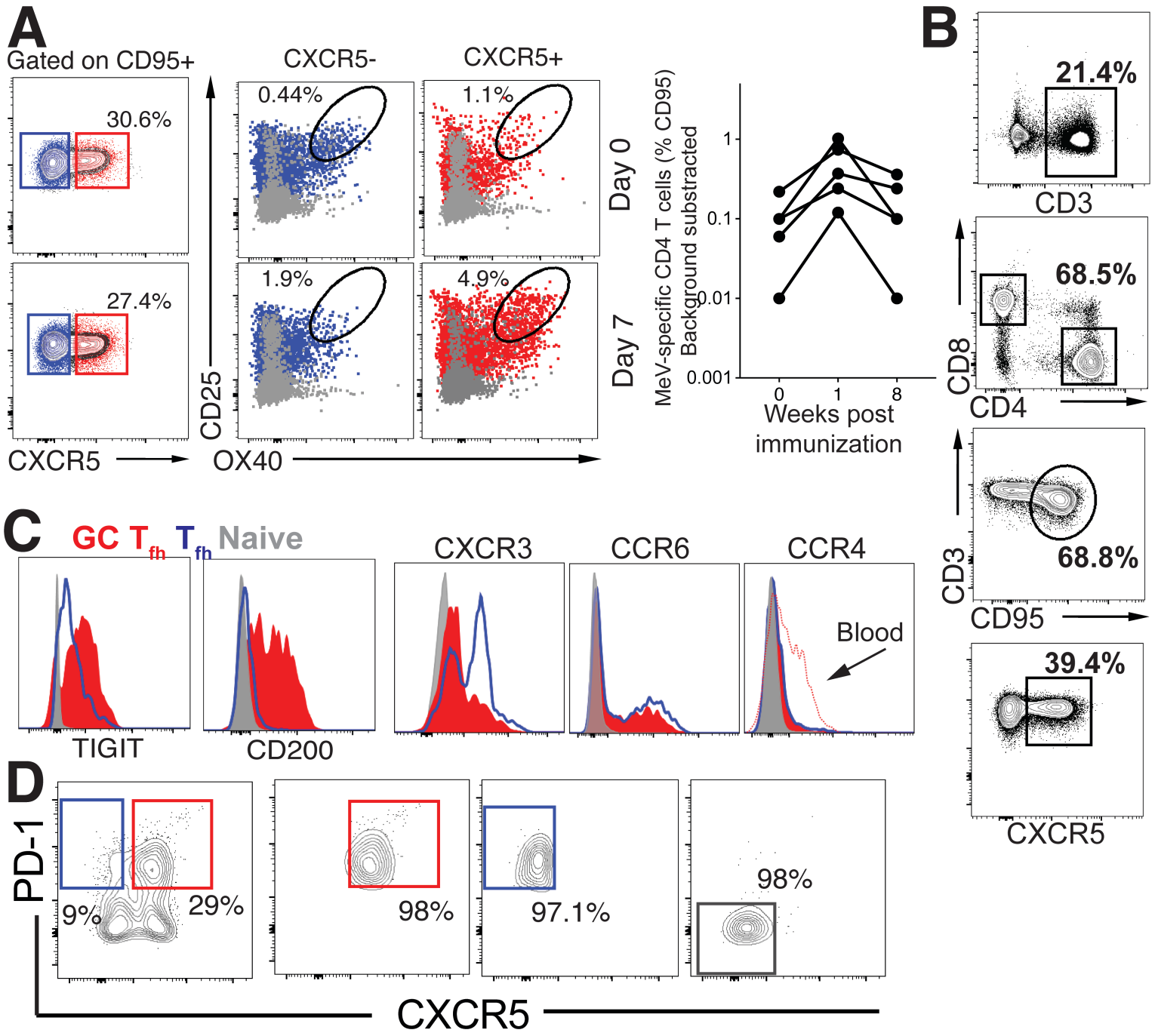

S2.

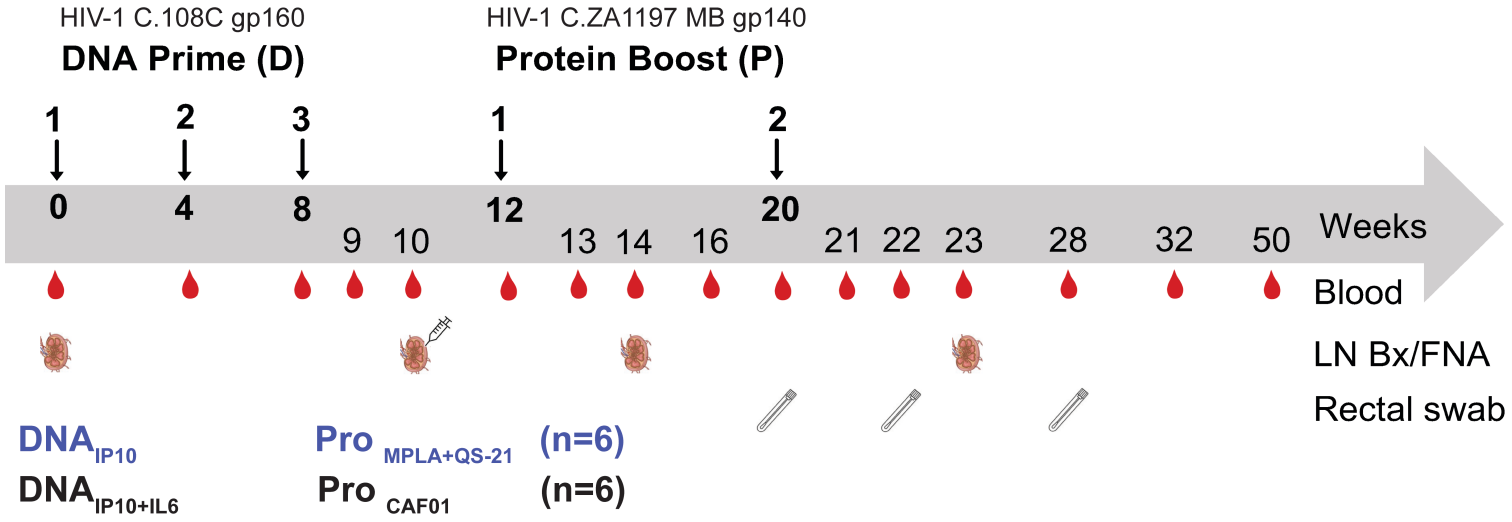
HIV-1 C.108C gp160
DNA Prime (D)
HIV-1 C.ZA1197 MB gp140
Protein Boost (P)
1
2
3
1
2
0
4
8
9
10
12
13
14
16
20
21
22
23
28
32
50
Weeks
Blood
LN Bx/FNA
Rectal swab
DNA IP10
DNA IP10+IL6
Pro MPLA+QS-21 (n=6)
Pro CAF01 (n=6)

S3, Supplement to Figure 2

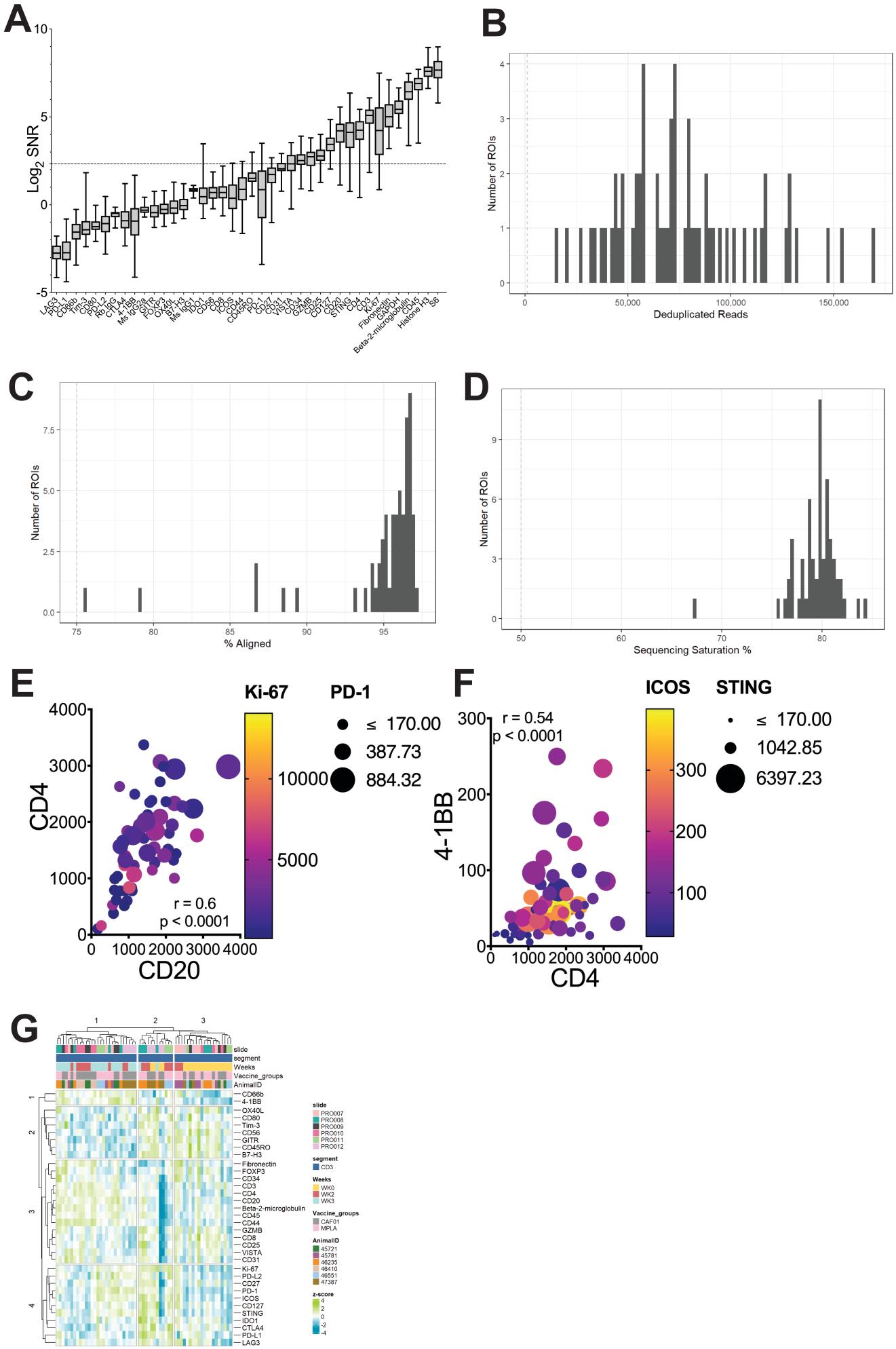

S4, Supplement to Figure 3

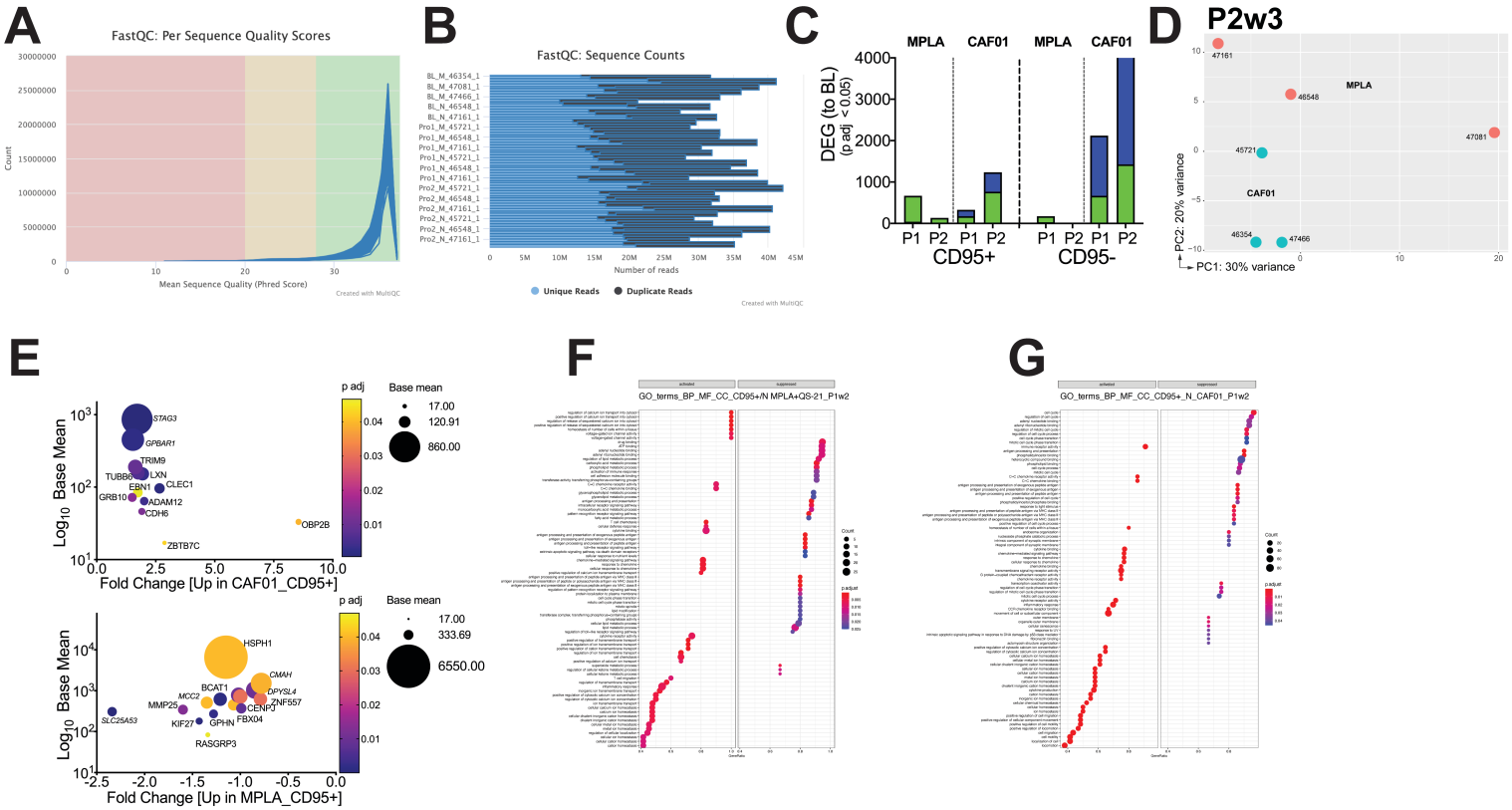

S5, Supplement to Figure 4

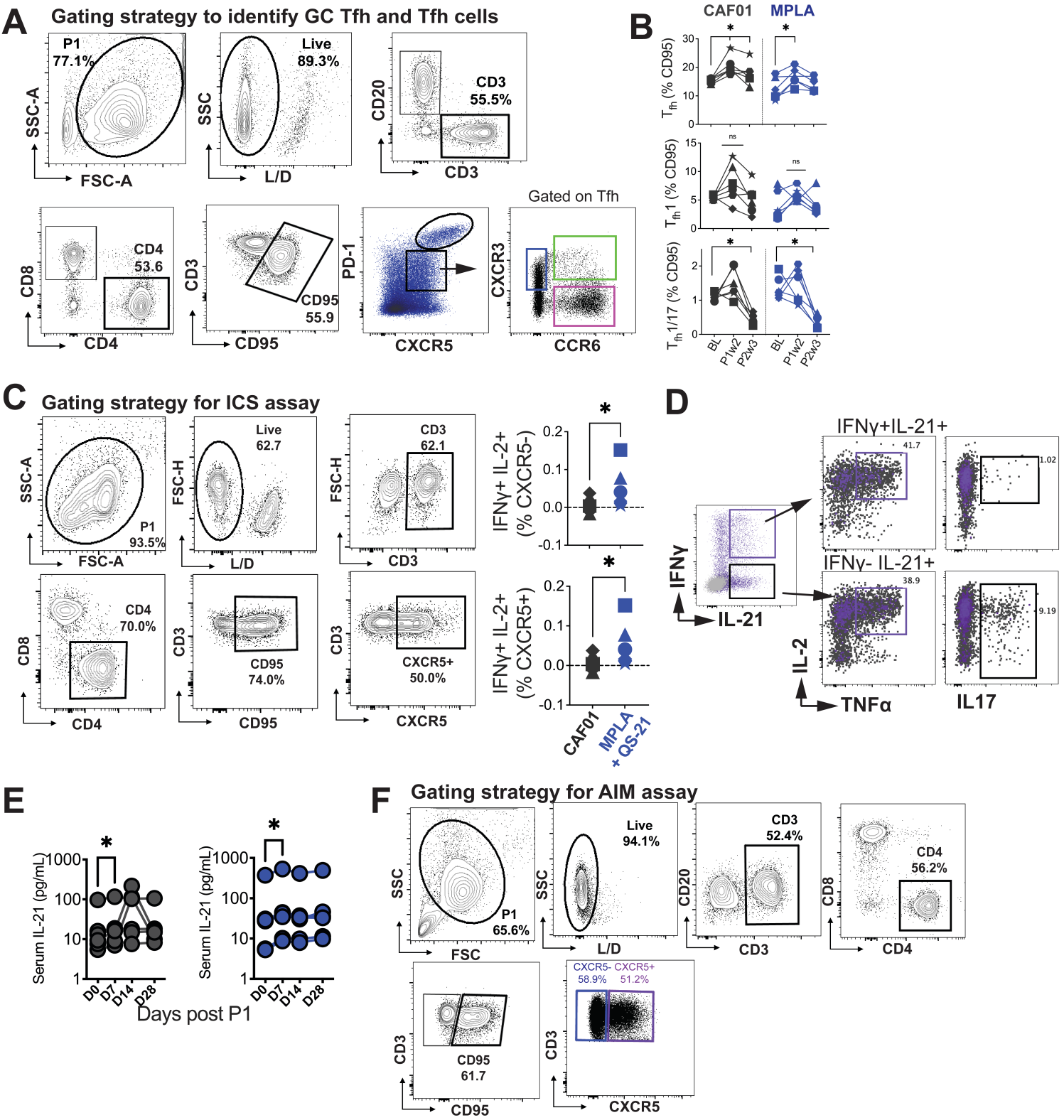

S6, Supplement to Figure 6

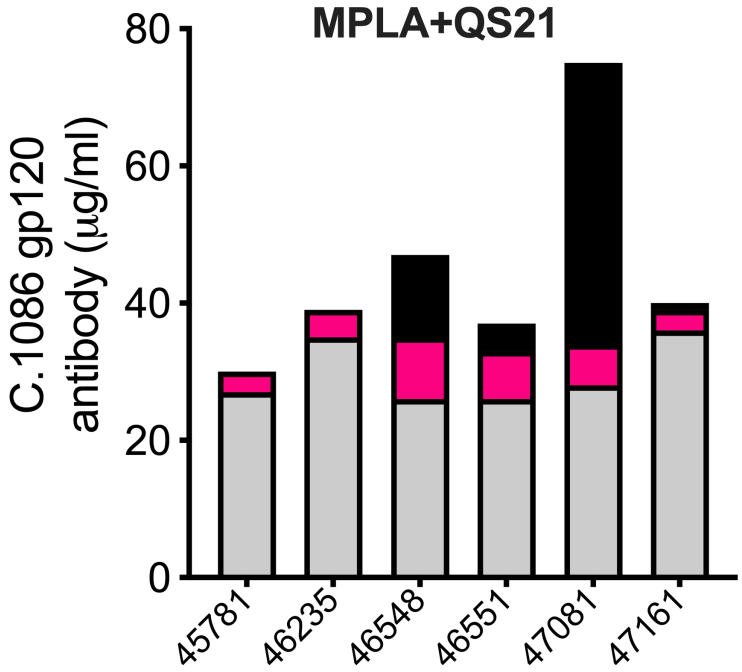

	IgG1	IgG2	IgG4
Number of values	6	6	6
Minimum	26.00	3.000	0.000
25% Percentile	26.00	3.000	0.000
Median	27.50	5.000	2.500
75% Percentile	35.25	7.500	19.25
Maximum	36.00	9.000	41.00
Range	10.00	6.000	41.00

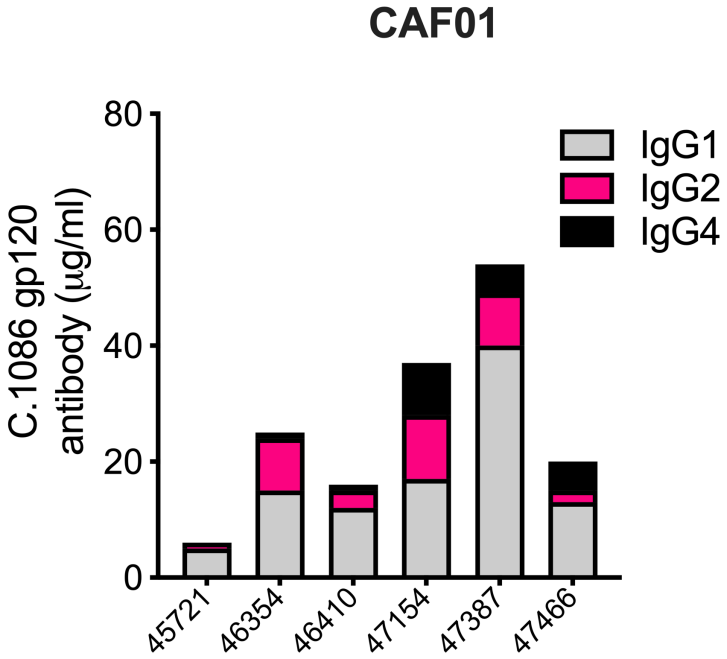

	IgG1	IgG2	IgG4
Number of values	6	6	6
Minimum	5.000	1.000	0.000
25% Percentile	10.25	1.750	0.7500
Median	14.00	6.000	3.000
75% Percentile	22.75	9.500	6.000
Maximum	40.00	11.00	9.000
Range	35.00	10.00	9.000
Mean	17.00	5.833	3.500
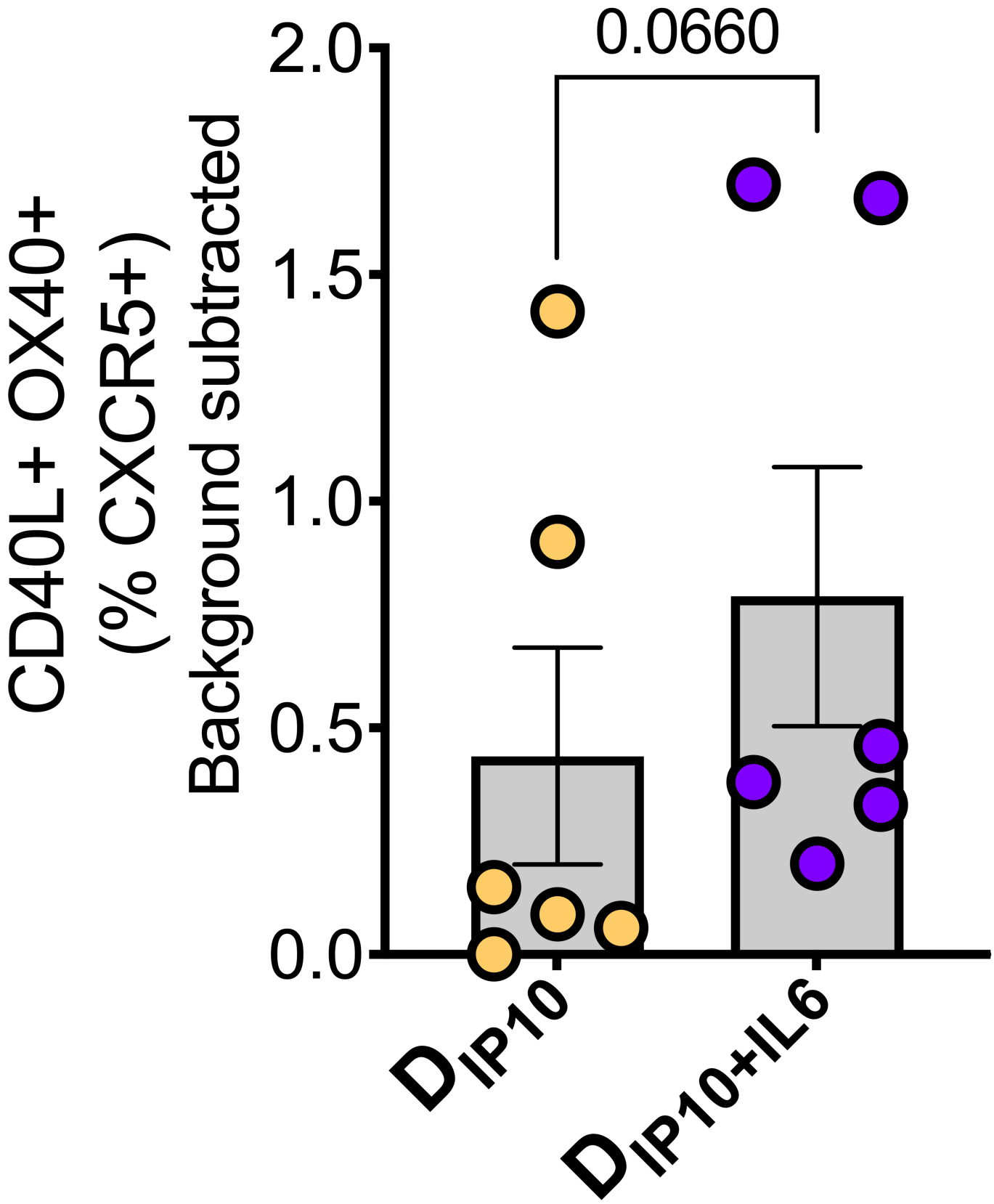
S7, Supplement to Figure 7